

# Estimating Transient Stability Regions of Large-scale Power Systems Part II: Reduced-order Stability Region with Computational Efficiency

Yuqing Lin, Tianhao Wen, Lei Chen, Yang Liu, *Member, IEEE, Member, CSEE*,  
and Q. H. Wu, *Life Fellow, IEEE, Fellow, CSEE*

**Abstract**—Part II of this paper presents a reduced-order stability region (ROSR) based method to estimate the full-order stability region (FOSR) of a large-scale power system. First, we introduce the definitions of FOSR and ROSR, followed by a comprehensive theory that reveals the relationships between them. Since the full-order system can be rewritten as a standard two timescale model and the reduced-order system is regarded as the slow subsystem of it, the proposed theory is derived based on the idea of singular perturbation. With rigorous mathematical proof, the properties of FOSR and ROSR are revealed. Moreover, a modified Energy Augmented Dynamic (EAD) algorithm and a constrained equidistant projection (CEP) approach are employed to estimate the ROSR and FOSR, respectively. The modified EAD algorithm and CEP form a so-called reduced-order stability region mapping (ROSRM) method. Finally, the proposed ROSRM method is applied to the IEEE 10-machine-39-bus power system, and simulation studies confirm its superiority to the traditional energy function method in terms of computational speed and reliability of results.

**Index Terms**—Large-scale power system, singular perturbation theory, stability region, sum of squares, transient stability.

## I. INTRODUCTION

**T**RANSIENT stability analysis investigates the dynamic behavior of power systems after large disturbances, which is of great significance in power system planning, operation, and control [1], [2]. Stability region (SR), mathematically known as *domain of attraction*, provides a quantitative description of transient stability [3]. It is defined as an invariant set such that all trajectories from points in the set converge to a corresponding asymptotically stable equilibrium point [4]. However, calculating an entire SR is a challenging task. In particular, for a large-scale power system, no one has yet been able to realize the derivation of an entire SR, because the dynamical model of the power system is high-dimensional and complex [2]. Model reduction has emerged as the most promising solution [5]. In this paper, we will present a work

on estimation of SRs for large-scale power systems based on reduced-order models. Our work is presented in two parts. Part I introduces how to capture the nonlinear dynamics of a power system by Koopman operator and derive a low-order dynamical model with reasonable accuracy. Part II describes how to use the reduced-order model combined with sum-of-squares (SOS) programming to approximate a reduced-order stability region (ROSR) and map it to the full-order state space to estimate the full-order stability region (FOSR). Below, we focus on the second part of our work.

Generally, the estimate of a SR is characterized by the level sets of a Lyapunov function. For small-scale power systems, several Lyapunov function based methods have been successfully applied [6], including the energy function method [2], [3], [7], [8], Lur'e type Lyapunov function method [9], [10], SOS based method [11]–[13] and extended Lyapunov function method [14], etc. However, these methods are inapplicable in large-scale power systems, due to the difficulties and computational complexity in constructing Lyapunov functions and approximating SRs [6]. Nonetheless, to address such a challenge, the energy function method attempts to construct numerical energy functions and estimate the local relevant boundary of a SR rather than the entire SR. This idea has inspired many approaches such as CUEP [15], PEBS [16] and BCU [17], but their application to large-scale systems is remains suboptimal [18], [19]. Besides, paper [6] introduces a class of connective stability based methods, including the vector/composite Lyapunov function method [20], [21], dissipative system theory [22] and input-to-state stability theory [23]. Unfortunately, the strongly-coupled characteristic of power systems brings enormous challenges to the implementation of these methods [6]. Consequently, until now, there has been no feasible method to calculate the entire SR of a large-scale power system.

In order to address this challenge, we utilize model reduction to drastically reduce the computational effort. However, the approach produces a new challenge of exploring the stability relationship between the reduced-order model and full-order model. Starting from the Koopman theory introduced in Part I, we rewrite the full-order system as a *standard two timescale model* and the reduced-order system can be regarded as the slow subsystem of it. Then *singular perturbation theory* [21, p.424] is able to build a bridge to analyze the stability relationship between these two systems. Although standard

Manuscript received February 18, 2024; revised May 23, 2024; accepted June 22, 2024. Date of online publication January 10, 2025; date of current version January 15, 2025.

Y. Q. Lin, T. H. Wen (corresponding author, email: epwentianhao@scut.edu.cn), L. Chen, Y. Liu, and Q. H. Wu are with the School of Electric Power Engineering, South China University of Technology, Guangzhou 510640, China.

DOI: 10.17775/CSEEJPES.2024.01180

two timescale model has been studied by singular perturbation theory in [21], [24]–[26], those papers either concentrate only on specific trajectories, or add impractical assumptions such as the existence of analytic energy function. Thus, it is required to improve the existing theory for analyzing the standard two timescale model.

The contribution of Part II is threefold.

(a) A complete theory is presented to analyze the stability of the full-order model and reduced-order model, with rigorous mathematical proofs. By introducing a thorough analysis of the standard two timescale model, the proposed theory reveals the correspondence between the trajectory convergence behavior in the FOSR and ROSR, respectively.

(b) Based on our previous work [13], a modified EAD algorithm is proposed to estimate the ROSR. Then we recast the obtained ROSR to the full-order state space to approximate the FOSR, by introducing *constrained equidistant projection* (CEP). The modified EAD algorithm and CEP form a so-called reduced-order stability region mapping (ROSRM) method.

(c) The proposed ROSRM method is applied to the IEEE 10-machine-39-bus power system case. The estimated FOSR is compared with that obtained by the traditional energy function method. Furthermore, we employ time domain simulation to verify the results.

In Part II of this paper, the concept and theory of reduced-order stability region are pioneered by us and successfully applied to large-scale power systems. Our work will open up a completely new research direction for transient stability analysis of modern power systems.

**Notation:** The set of  $n \times m$  real and complex matrices are represented by  $\mathbb{R}^{n \times m}$  and  $\mathbb{C}^{n \times m}$  respectively. The set of polynomials and SOS polynomials defined in  $x \in \mathbb{R}^n$  are denoted by  $\mathbb{P}_n[x]$  and  $\mathbb{S}_n[x]$ , respectively.  $\text{col}(\mathbf{T})$  denotes the columns of matrix  $\mathbf{T}$ .  $\mathbf{T}^+$  is the Moore-Penrose pseudoinverse of matrix  $\mathbf{T}$ .  $\mathbb{R}_{\geq 0} := [0, +\infty)$ ,  $\mathbb{R}_{< 0} := (-\infty, 0)$ ,  $\mathbb{C}_- := \{p \in \mathbb{C} | \text{Re}(p) < 0\}$ . For  $p \in \mathbb{C}$ ,  $\text{Re}(p)$  is the real part of  $p$ ,  $\text{Im}(p)$  is the imaginary part of  $p$ ,  $p^*$  is the conjugate of  $p$ . For a set  $A$ ,  $\text{int}(A)$  is the interior of  $A$ ,  $\partial A$  is the boundary of  $A$ . For a map  $M : A \rightarrow B$ , we say that  $M \in C^0(A; B)$  if  $M$  is continuous in  $A$ . We say that  $M \in C^k(A; B)$  ( $k \geq 1$ ) if  $M$  has  $k$ -th-order continuous partial derivatives in  $A$ .  $\mathbf{I}_n$  is the identity matrix of size  $n \times n$ ,  $\mathbf{O}_m$  is the zero matrix of size  $m \times m$ . Given matrices  $\mathbf{A}_1, \mathbf{A}_2, \dots, \mathbf{A}_q$ ,  $\text{blkdiag}(\mathbf{A}_1, \mathbf{A}_2, \dots, \mathbf{A}_q)$  is the block-diagonal matrix with diagonal blocks  $\mathbf{A}_1, \mathbf{A}_2, \dots, \mathbf{A}_q$ . For a matrix  $\mathbf{A} \in \mathbb{C}^{n \times n}$ ,  $\text{Ln}(\mathbf{A})$  is the *logarithm* of  $\mathbf{A}$  [27, p.65]. For  $\mathbf{q} \in \mathbb{R}^k$ ,  $\mathbb{B}_k(\mathbf{q}, \rho)$  is the  $k$ -dimensional close ball centered at  $\mathbf{q}$  with radius  $\rho$ .

## II. STABILITY ANALYSIS OF THE FULL-ORDER MODEL AND REDUCED-ORDER MODEL

### A. Full-order Stability Region and Reduced-order Stability Region

Suppose that the full-order model is a continuous-time, autonomous and nonlinear dynamical system:

$$\frac{d\mathbf{x}(t)}{dt} = \mathbf{f}(\mathbf{x}(t)) \quad (1)$$

where  $\mathbf{x} \in \mathbb{R}^n$ ,  $\mathbf{f} : \mathbb{R}^n \rightarrow \mathbb{R}^n$  and  $\mathbf{x} = [x_1, x_2, \dots, x_n]^\top$ . Assume that  $\mathbf{x} = \mathbf{0}$  is an equilibrium point, i.e.  $\mathbf{f}(\mathbf{0}) = \mathbf{0}$ . Define a finite time- $t$  flow  $\mathbf{S}(t, \mathbf{x}(t_0)) : \mathbf{x}(t_0) \rightarrow \mathbf{x}(t_0 + t) = \mathbf{x}(t_0) + \int_{t_0}^{t_0+t} \mathbf{f}(\mathbf{x}(\tau)) d\tau$ . If  $\mathbf{x} = \mathbf{0}$  is an asymptotically stable equilibrium point (ASEP), the corresponding stability region (SR) is defined as:

$$\mathcal{D} = \{\mathbf{x}(0) \in \mathbb{R}^n | \lim_{t \rightarrow \infty} \mathbf{S}(t, \mathbf{x}(0)) = \mathbf{0}\} \quad (2)$$

We refer to  $\mathcal{D}$  as the full-order stability region (FOSR) of system (1).

According to the Lyapunov stability theory [2], [4], [13], if there exist an open set  $\Omega \subseteq \mathbb{R}^n$  and a continuously differentiable function  $V(x) : \Omega \rightarrow \mathbb{R}$ , called Lyapunov function, such that

$$\begin{aligned} V(\mathbf{0}) &= 0, V(\mathbf{x}) > 0, \quad \forall \mathbf{x} \in \Omega \setminus \{\mathbf{0}\} \\ \dot{V}(\mathbf{0}) &= 0, \dot{V}(\mathbf{x}) < 0, \quad \forall \mathbf{x} \in \Omega \setminus \{\mathbf{0}\} \end{aligned} \quad (3)$$

then a set  $D = \{\mathbf{x} | V(\mathbf{x}) \leq c, c > 0\} \subset \Omega$  is guaranteed to be an invariant subset of the FOSR with respect to  $\mathbf{x} = \mathbf{0}$ .  $D$  can be regarded as an estimate of  $\mathcal{D}$ , called the estimated FOSR.

As for the reduced-order model of system (1), we recall the relevant work in Part I of this paper. Assume that a transformation matrix  $\mathbf{T}$  can be found to make

$$\mathbf{x} \approx \mathbf{T}\mathbf{z} \quad (4)$$

where  $\mathbf{T} \in \mathbb{R}^{n \times r}$ ,  $\mathbf{z} \in \mathbb{R}^r$  and  $r < n$ . Then, by the Galerkin projection method [28], one can derive a reduced-order model:

$$\frac{d\mathbf{z}}{dt} = \mathbf{T}^+ \mathbf{f}(\mathbf{T}\mathbf{z}) \triangleq \mathbf{g}(\mathbf{z}). \quad (5)$$

Reduced-order model (5) evolves in  $\mathbb{R}^r$  and approximates the dynamics of full-order model (1) in some sense. Similarly, assume  $\mathbf{z} = \mathbf{0}$  is an ASEP and define a finite time- $t$  flow  $\hat{\mathbf{S}}(t, \mathbf{z}(t_0)) : \mathbf{z}(t_0) \rightarrow \mathbf{z}(t_0 + t) = \mathbf{z}(t_0) + \int_{t_0}^{t_0+t} \mathbf{g}(\mathbf{z}(\tau)) d\tau$ . Then the reduced-order stability region (ROSR) can be defined as:

$$\hat{\mathcal{D}} = \{\mathbf{z}(0) \in \mathbb{R}^r | \lim_{t \rightarrow \infty} \hat{\mathbf{S}}(t, \mathbf{z}(0)) = \mathbf{0}\}. \quad (6)$$

From the Lyapunov stability theory, if there exist  $\hat{\Omega} \subseteq \mathbb{R}^r$  and  $\hat{V}(z) : \hat{\Omega} \rightarrow \mathbb{R}$ , such that

$$\begin{aligned} \hat{V}(\mathbf{0}) &= 0, \hat{V}(\mathbf{z}) > 0, \quad \forall \mathbf{z} \in \hat{\Omega} \setminus \{\mathbf{0}\} \\ \dot{\hat{V}}(\mathbf{0}) &= 0, \dot{\hat{V}}(\mathbf{z}) < 0, \quad \forall \mathbf{z} \in \hat{\Omega} \setminus \{\mathbf{0}\} \end{aligned} \quad (7)$$

then a set  $\hat{D} = \{\mathbf{z} | \hat{V}(\mathbf{z}) \leq \hat{c}, \hat{c} > 0\} \subset \hat{\Omega}$  is an invariant subset of  $\hat{\mathcal{D}}$  and can be called the estimated ROSR.

Note that  $\mathcal{D}$  and  $\hat{\mathcal{D}}$  are not topologically conjugate because they have different dimensions. In practice, we are interested in  $D$  rather than  $\hat{D}$ . However,  $\hat{D}$  is easier to compute and can be employed to deduce the desired  $D$ .

### B. Mapping Relationships Between the Full-order Space and Reduced-order Space

**Definition 1.** Given a set  $\mathcal{Q} \subseteq \mathbb{R}^r$  and a transformation  $\mathbf{x} = \mathbf{T}\mathbf{z}$  with  $\mathbf{x} \in \mathbb{R}^n$ ,  $\mathbf{z} \in \mathbb{R}^r$ , we define  $\mathcal{S} \triangleq \{\mathbf{x}_s | \mathbf{x}_s = \mathbf{T}\mathbf{z}_q, \mathbf{z}_q \in \mathcal{Q}\} \subseteq \mathbb{R}^n$  and  $\mathcal{P} \triangleq \{\mathbf{x}_p | \frac{\langle \mathbf{x}_p, \mathbf{x}_s \rangle}{\|\mathbf{x}_s\|} = \|\mathbf{x}_s\|, \mathbf{x}_s \in \mathcal{S}\} \subseteq \mathbb{R}^n$ , i.e.  $\mathcal{P}$  is the normal bundle of  $\mathcal{S}$ .

**Theorem 1.** Given a set  $\mathcal{Q} \subseteq \mathbb{R}^r$  and a transformation  $\mathbf{x} = \mathbf{T}\mathbf{z}$ , we have the sets  $\mathcal{S}$  and  $\mathcal{P}$  based on Definition 1. Then there exist a bijective map between  $\mathcal{S}$  and  $\mathcal{Q}$ , an injective map from  $\mathcal{Q}$  to  $\mathcal{P}$ , and a surjective map from  $\mathcal{P}$  to  $\mathcal{Q}$ .

*Proof:* In the first place, since  $\mathbf{T} \in \mathbb{R}^{n \times r}$ ,  $\text{rank}(\mathbf{T}) = r$  and  $r < n$ ,  $\mathbf{T}^+\mathbf{T} = \mathbf{I}_r$ , where  $\mathbf{T}^+ = (\mathbf{T}^\top\mathbf{T})^{-1}\mathbf{T}^\top$ . Thus  $\mathbf{T}$  is an injective map from  $\mathbb{R}^r$  to  $\mathbb{R}^n$ . As  $\mathcal{Q} \subseteq \mathbb{R}^r$  and  $\mathcal{S} = \mathbf{T}(\mathcal{Q}) \subseteq \mathcal{P}$ ,  $\mathbf{T}$  also induces an injective map from  $\mathcal{Q}$  to  $\mathcal{P}$ . In addition,  $\forall \mathbf{x}_{s0} \in \mathcal{S}$ , it is obvious that  $\exists \mathbf{z}_{q0} \in \mathcal{Q}$ , s.t.  $\mathbf{x}_{s0} = \mathbf{T}\mathbf{z}_{q0}$  and  $\mathbf{z}_{q0} = \mathbf{T}^+\mathbf{x}_{s0} = \mathbf{T}^+\mathbf{T}\mathbf{z}_{q0}$ . As a result,  $\mathbf{T}$  is a surjective map from  $\mathcal{Q}$  to  $\mathcal{S}$ . But because  $\mathbf{T}$  is also injective,  $\mathbf{T}$  is actually a bijective map between  $\mathcal{S}$  and  $\mathcal{Q}$ . Moreover,  $\forall \mathbf{x}_{p1} \in \mathcal{P}$ , according to the theory of orthonormal decomposition [29],  $\exists$  unique  $\mathbf{x}_{s1} \in \mathcal{S}$  and  $\mathbf{x}_{g1} \in (\text{span}\{\text{col}(\mathbf{T})\})^\perp$ , where  $(\text{span}\{\text{col}(\mathbf{T})\})^\perp$  is the orthonormal complement of  $\text{span}\{\text{col}(\mathbf{T})\}$ , s.t.  $\mathbf{x}_{p1} = \mathbf{x}_{s1} + \mathbf{x}_{g1}$ . Then we have  $\mathbf{T}^+\mathbf{x}_{p1} = \mathbf{T}^+\mathbf{x}_{s1} + \mathbf{T}^+\mathbf{x}_{g1} = \mathbf{T}^+\mathbf{x}_{s1} + (\mathbf{T}^\top\mathbf{T})^{-1}\mathbf{T}^\top\mathbf{x}_{g1} = \mathbf{T}^+\mathbf{x}_{s1} = \mathbf{z}_{q1}$ , i.e.,  $\mathbf{z}_{q1} = \mathbf{T}^+\mathbf{x}_{p1}$ . Note that  $\mathbf{z}_{q1} \in \mathcal{Q}$ . Finally,  $\forall \mathbf{z}_{q2} \in \mathcal{Q}$ ,  $\mathbf{T}\mathbf{z}_{q2} \in \mathcal{S} \subseteq \mathcal{P}$  and  $\mathbf{T}^+\mathbf{T}\mathbf{z}_{q2} = \mathbf{z}_{q2}$ . Therefore,  $\mathbf{T}^+$  is a surjective map from  $\mathcal{P}$  to  $\mathcal{Q}$ .  $\square$

From Theorem 1 and its proof, we conclude the mapping relationships among  $\mathcal{Q}$ ,  $\mathcal{S}$  and  $\mathcal{P}$ :

$$\mathbf{x}_s = \mathbf{T}\mathbf{z}_q, \mathbf{z}_q = \mathbf{T}^+\mathbf{x}_s, \mathbf{z}_q = \mathbf{T}^+\mathbf{x}_p \quad (8a)$$

$$\mathbf{x}_s = \mathbf{T}\mathbf{T}^+\mathbf{x}_p, \mathbf{x}_p = \mathbf{x}_s + \mathbf{x}_g, \mathbf{T}^\top\mathbf{x}_g = \mathbf{0} \quad (8b)$$

$$\forall \mathbf{z}_q \in \mathcal{Q}, \mathbf{x}_s \in \mathcal{S}, \mathbf{x}_p \in \mathcal{P}$$

The relationships are also shown in Fig. 1. Note that  $\mathbf{z}_q = \mathbf{T}^+\mathbf{x}_s = \mathbf{T}^+\mathbf{x}_p$  and  $\mathcal{S} \subset \mathcal{P}$ , which illustrates that the map from  $\mathcal{P}$  to  $\mathcal{Q}$  is many-to-one. If  $\mathcal{Q} = \hat{D}$  is the estimated ROSR,  $\mathcal{P}$  is not the estimated FOSR  $D$ . This is because  $\mathcal{P}$  is unbounded, even though all points in  $\mathcal{P}$  can be projected into  $\mathcal{Q}$ . Nonetheless, there exists a  $D$  satisfying  $D \subset \mathcal{P}$ .

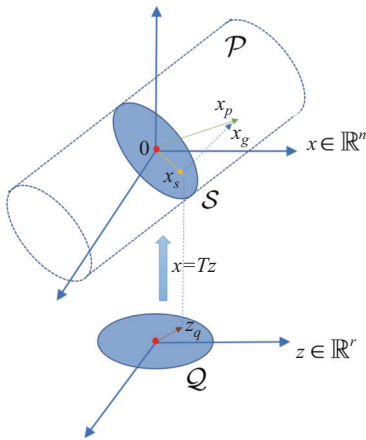


Fig. 1. Mapping relationships among the sets defined in the full-order space and reduced-order one.

Furthermore, if set  $\mathcal{Q}$  is expanded to the entire space, i.e.  $\mathcal{Q} = \mathbb{R}^r$ , set  $\mathcal{S}$  is actually a  $r$ -dimensional unbounded manifold defined in  $\mathbb{R}^n$  and  $\mathcal{P} = \mathbb{R}^n$ . The above-mentioned mapping relationships remain unchanged.

### C. Rewrite the Full-order Model as a Standard Two Timescale Model

As has been discussed in Part I of this paper, the solution of (1) initiated at a given point  $\mathbf{x}(0) \in \mathcal{D}$  can be expressed as the linear combination of Koopman eigenfunctions of the system, that is,  $\forall t \geq 0$ ,

$$\mathbf{x}(t) = \mathbf{S}(t, \mathbf{x}(0)) = \sum_{i=1}^{+\infty} \eta_i(\mathbf{x}(t)) \zeta_i = \sum_{i=1}^{+\infty} e^{\lambda_i t} \eta_i(\mathbf{x}(0)) \zeta_i \quad (9)$$

where  $\eta_i (i = 1, 2, \dots) : \mathbb{R}^n \rightarrow \mathbb{C}$  are Koopman eigenfunctions satisfying  $\eta_i(\mathbf{x}(t)) = e^{\lambda_i t} \eta_i(\mathbf{x}(0))$ ,  $\lambda_i \in \mathbb{C}_-$  is the  $i$ th Koopman eigenvalue, and  $\zeta_i \in \mathbb{C}^n$  is the  $i$ th Koopman mode. Suppose that the real part of  $\lambda_i$  decreases as index  $i$  increases. And, the first  $c$  (usually  $c \geq n$ ) Koopman eigenvalues, together with their associated Koopman eigenfunctions and Koopman modes, determine the general dynamic behavior of (1) and can be obtained via PMK-DMD algorithm proposed in Part I. For the purpose of model order reduction, the realization process mentioned in Part I is performed on  $\lambda_i, \eta_i, \zeta_i (i = 1, \dots, c)$ , so that (9) can be rewritten as:

$$\begin{aligned} \mathbf{x}(t) &= \underline{\Theta}_p \underline{\Lambda}_p(t) \underline{\eta}_p(\mathbf{x}(0)) + \text{errs} \\ &= \underline{\Theta}_p \underline{\eta}_p(\mathbf{x}(t)) + \text{errs} \end{aligned} \quad (10)$$

where  $\underline{\Theta}_p$  has been shown in Part I,  $\underline{\eta}_p(\mathbf{x}) = [\text{Re}\{\eta_1(\mathbf{x})\}, \text{Im}\{\eta_1(\mathbf{x})\}, \dots, \text{Re}\{\eta_{c_1}(\mathbf{x})\}, \text{Im}\{\eta_{c_1}(\mathbf{x})\}, \eta_{2c_1+1}(\mathbf{x}), \dots, \eta_c(\mathbf{x})]^\top$ ,

$$\begin{aligned} \underline{\Lambda}_p(t) &= \text{blkdiag} \left( \begin{bmatrix} e^{\nu_1 t} \cos(\varsigma_1 t) & -e^{\nu_1 t} \sin(\varsigma_1 t) \\ e^{\nu_1 t} \sin(\varsigma_1 t) & e^{\nu_1 t} \cos(\varsigma_1 t) \end{bmatrix}, \dots, \right. \\ &\quad \left. \begin{bmatrix} e^{\nu_{c_1} t} \cos(\varsigma_{c_1} t) & -e^{\nu_{c_1} t} \sin(\varsigma_{c_1} t) \\ e^{\nu_{c_1} t} \sin(\varsigma_{c_1} t) & e^{\nu_{c_1} t} \cos(\varsigma_{c_1} t) \end{bmatrix}, e^{\lambda_{2c_1+1} t}, \dots, e^{\lambda_c t} \right) \end{aligned}$$

$\nu_k = \text{Re}\{\lambda_{2k-1}\} (k = 1, \dots, c_1)$ ,  $\varsigma_k = \text{Im}\{\lambda_{2k-1}\}$ ,  $\lambda_{2k} = \lambda_{2k-1}^*$ , and  $\text{errs}$  contains fast decaying terms related to  $\lambda_m, \eta_m, \zeta_m (m > c)$ . Note that for ease of discussion, we assume here that  $\lambda_1, \dots, \lambda_{2c_1}$  are complex eigenvalues and  $\lambda_{2c_1+1}, \dots, \lambda_c \in \mathbb{R}_{<0}$ .

Now suppose further that system (1) possesses two timescale dynamics. Specifically, the real part of Koopman eigenvalues  $\lambda_l (l = r+1, \dots, c)$  are significantly smaller than that of  $\lambda_q (q = 1, \dots, r)$ , where  $r < \min\{n, c\}$ , indicating that  $\eta_{r+1}, \dots, \eta_c$  decay faster than  $\eta_1, \dots, \eta_r$ . This motivates the construction of reduced-order model (5), with matrix  $\mathbf{T}$  composed of the 1 st~ $r$ th column of  $\underline{\Theta}_p$ . To analyze the dynamic relations between (1) and (5), we first define

$$\begin{aligned} \bar{\omega}_s &= [\mathbf{I}_r, \mathbf{O}_{c-r}] \underline{\eta}_p(\mathbf{x}) \bar{\omega}_f = [\mathbf{O}_c, \mathbf{I}_{c-r}] \underline{\eta}_p(\mathbf{x}) \\ \mathbf{T}_s &= \underline{\Theta}_p [\mathbf{I}_r, \mathbf{O}_{c-r}]^\top \mathbf{T}_f = \underline{\Theta}_p [\mathbf{O}_c, \mathbf{I}_{c-r}]^\top \end{aligned}$$

Then, let  $\mathbf{T} = \mathbf{T}_s$  in (4), and from (10) we have

$$\begin{aligned} \mathbf{x} &= \mathbf{T}_s \bar{\omega}_s + \mathbf{T}_f \bar{\omega}_f + \text{errs} \\ \mathbf{z} &= \mathbf{T}_s^+ \mathbf{x} = \bar{\omega}_s + \mathbf{T}_s^+ \mathbf{T}_f \bar{\omega}_f + \text{errs} \end{aligned} \quad (11)$$

Furthermore, from (11), we rewrite  $\mathbf{x}$  as:

$$\mathbf{x} = \mathbf{T}_s \mathbf{z} + \mathbf{T}_s (\bar{\omega}_s - \mathbf{z}) + \mathbf{T}_f \bar{\omega}_f + \text{errs}$$

$$\begin{aligned} &= \mathbf{T}_s \mathbf{z} + \mathbf{T}_f \bar{\boldsymbol{\omega}}_f - \mathbf{T}_s \mathbf{T}_s^+ \mathbf{T}_f \bar{\boldsymbol{\omega}}_f + \text{errs} \\ &= \mathbf{T}_s \mathbf{z} + (\mathbf{I}_n - \mathbf{T}_s \mathbf{T}_s^+) \mathbf{T}_f \bar{\boldsymbol{\omega}}_f + \text{errs} \end{aligned} \quad (12)$$

If  $|\operatorname{Re}\{\lambda_l\}| (l = r+1, \dots, c)$  is of the order of  $1/\epsilon$ , where  $\epsilon$  is a small positive constant playing the same role as the small parameter in the standard two timescale model in singular perturbation theory [21, p.424], then the dynamics of (1) within  $\mathcal{D}$  can also be described by

$$\begin{cases} \frac{d\mathbf{z}}{dt} = \mathbf{T}_s^+ \mathbf{f}(\mathbf{T}_s \mathbf{z} + (\mathbf{I}_n - \mathbf{T}_s \mathbf{T}_s^+) \mathbf{T}_f \bar{\boldsymbol{\omega}}_f + \text{errs}) \\ \frac{d\bar{\boldsymbol{\omega}}_f}{dt} = \frac{1}{\epsilon} \boldsymbol{\Xi} \bar{\boldsymbol{\omega}}_f \end{cases} \quad (13)$$

where  $\frac{1}{\epsilon} \boldsymbol{\Xi} = \frac{1}{t} \operatorname{Ln}([\mathbf{O}_c, \mathbf{I}_{c-r}] \mathbf{A}_p(t) [\mathbf{O}_c, \mathbf{I}_{c-r}]^\top)$ . It can be proved that  $\boldsymbol{\Xi}$  is a *Hurwitz* matrix and actually irrelevant of  $t$ . With the term *errs* neglected since it decays extremely fast, (13) has the form of standard two timescale model. Also, by setting  $\bar{\boldsymbol{\omega}}_f$  to 0, we can find out that (5) is the *slow subsystem* [21, p.424] of (13).

Taking the similarity between (13) and standard two timescale model into consideration, we will utilize several properties of the standard model to establish the links between the dynamics of (1), (13) and (5).

#### D. Stability Analysis of a Standard Two Timescale Model

In the following, we will present a thorough analysis of a standard two-timescale model, focusing on the stability regions of the slow subsystem, fast subsystem and the entire model. Although standard two timescale model has been previously analyzed using singular perturbation theory in [21], [24], [25], those papers either concentrate only on specific trajectories, or add impractical assumptions such as the existence of analytic energy function.

Consider the standard two timescale model shown below,

$$\Sigma_\epsilon : \begin{cases} \frac{d\mathbf{x}}{dt} = \mathbf{f}(\mathbf{x}, \mathbf{y}) \\ \epsilon \frac{d\mathbf{y}}{dt} = \mathbf{g}(\mathbf{x}, \mathbf{y}) \end{cases} \quad (14)$$

where  $\mathbf{x} \in \mathbb{R}^n$ ,  $\mathbf{y} \in \mathbb{R}^m$ ,  $\mathbf{f} \in \mathcal{C}^2(\mathbb{R}^{n+m}; \mathbb{R}^n)$ ,  $\mathbf{g} \in \mathcal{C}^2(\mathbb{R}^{n+m}; \mathbb{R}^m)$ , and  $\epsilon$  is a sufficiently small positive parameter. Via the change of timescale  $\tau = t/\epsilon$ , (14) can be transformed into

$$\Pi_\epsilon : \begin{cases} \frac{d\mathbf{x}}{d\tau} = \epsilon \mathbf{f}(\mathbf{x}, \mathbf{y}) \\ \frac{d\mathbf{y}}{d\tau} = \mathbf{g}(\mathbf{x}, \mathbf{y}) \end{cases} \quad (15)$$

When  $\epsilon = 0$ , (15) becomes the fast subsystem (which is also called the *boundary-layer system* [24] of (14))

$$\Pi_0 : \begin{cases} \frac{d\mathbf{x}}{d\tau} = 0 \\ \frac{d\mathbf{y}}{d\tau} = \mathbf{g}(\mathbf{x}, \mathbf{y}) \end{cases} \quad (16)$$

Also, setting  $\epsilon = 0$  in (14), we can obtain the slow subsystem

$$\Sigma_0 : \begin{cases} \frac{d\mathbf{x}}{dt} = \mathbf{f}(\mathbf{x}, \mathbf{y}) \\ \mathbf{0} = \mathbf{g}(\mathbf{x}, \mathbf{y}) \end{cases} \quad (17)$$

Assume that (14) has a hyperbolic asymptotically stable equilibrium point  $(\mathbf{x}_s, \mathbf{y}_s)$  located in  $\Gamma$ , where

$$\Gamma : \left\{ (\mathbf{x}, \mathbf{y}) \in \mathbb{R}^{n+m} \mid \mathbf{g}(\mathbf{x}, \mathbf{y}) = \mathbf{0}, \operatorname{Re} \left\{ \operatorname{eig} \left( \frac{\partial \mathbf{g}}{\partial \mathbf{y}} \right) \right\} < 0 \right\}$$

The location and hyperbolicity of  $(\mathbf{x}_s, \mathbf{y}_s)$  ensure that it is also locally exponentially stable, with respect to (14) and (17). Denote  $\Gamma_s$  the connected component of  $\Gamma$  containing  $(\mathbf{x}_s, \mathbf{y}_s)$ ,  $\phi_{\Sigma_\epsilon}(t, (\mathbf{x}, \mathbf{y}))$  the solution of (14) initiated at  $(\mathbf{x}, \mathbf{y})$ ,  $\phi_{\Sigma_0}(t, (\mathbf{x}, \mathbf{y}))$  the solution of (17) starting at  $(\mathbf{x}, \mathbf{y})$ ,  $\phi_{\Pi_0}(\tau, (\mathbf{x}, \mathbf{y}))$  the solution of (16) initiated at  $(\mathbf{x}, \mathbf{y})$ ,  $\phi_{\Pi_\epsilon}(\tau, (\mathbf{x}, \mathbf{y}))$  the solution of (15) starting at  $(\mathbf{x}, \mathbf{y})$ ,

$$\begin{aligned} \mathcal{A}_\epsilon(\mathbf{x}_s, \mathbf{y}_s) &: \left\{ (\mathbf{x}, \mathbf{y}) \in \mathbb{R}^{n+m} \mid \lim_{t \rightarrow +\infty} \phi_{\Sigma_\epsilon}(t, (\mathbf{x}, \mathbf{y})) \right. \\ &= (\mathbf{x}_s, \mathbf{y}_s) \left. \right\} \end{aligned}$$

$$\begin{aligned} \mathcal{A}_0(\mathbf{x}_s, \mathbf{y}_s) &: \left\{ (\mathbf{x}, \mathbf{y}) \in \Gamma_s \mid \forall t \geq 0, \phi_{\Sigma_0}(t, (\mathbf{x}, \mathbf{y})) \in \Gamma_s \right. \\ &\wedge \lim_{t \rightarrow +\infty} \phi_{\Sigma_0}(t, (\mathbf{x}, \mathbf{y})) = (\mathbf{x}_s, \mathbf{y}_s) \left. \right\} \end{aligned}$$

$$\begin{aligned} \mathcal{A}_F(\mathbf{x}_0, \mathbf{y}^*) &: \left\{ (\mathbf{x}, \mathbf{y}) \in \mathbb{R}^{n+m} \mid \lim_{\tau \rightarrow +\infty} \phi_{\Pi_0}(\tau, (\mathbf{x}, \mathbf{y})) \right. \\ &= (\mathbf{x}_0, \mathbf{y}^*) \left. \right\} \end{aligned}$$

$$\mathcal{D}_0(\mathbf{x}_s, \mathbf{y}_s) \triangleq \bigcup_{0 < \epsilon^* < 1} \bigcap_{0 < \epsilon \leq \epsilon^*} \mathcal{A}_\epsilon(\mathbf{x}_s, \mathbf{y}_s)$$

As for (14), we will provide Theorem 2 and Theorem 3 to reveal the relations between its stability region and that of (15), (17). First, we briefly discuss the geometric properties of  $\Gamma_s$  and  $\mathcal{A}_0(\mathbf{x}_s, \mathbf{y}_s)$ .

**Lemma 1.**  $\Gamma_s$  is a path-connected regular submanifold of dimension  $n$  in  $\mathbb{R}^{n+m}$ . Also,  $\Gamma_s$  is equipped with an atlas consisting of only one coordinate chart  $(\Gamma_s, \tilde{\pi}_x)$ , with  $\tilde{\pi}_x : \Gamma_s \rightarrow \mathbb{R}^n$ . Moreover, there is a map  $\mathbf{h}_s \in \mathcal{C}^2(\tilde{\pi}_x(\Gamma_s); \mathbb{R}^m)$  satisfying  $\mathbf{g}(\mathbf{x}, \mathbf{h}_s(\mathbf{x})) = \mathbf{0}$  for all  $\mathbf{x} \in \tilde{\pi}_x(\Gamma_s)$ . See [30] [25, CH.7] for more details.

**Lemma 2.**  $\mathcal{A}_0(\mathbf{x}_s, \mathbf{y}_s)$  is a positively invariant set open in  $\Gamma_s$ . That is,  $\forall (\mathbf{x}, \mathbf{y}) \in \mathcal{A}_0(\mathbf{x}_s, \mathbf{y}_s)$ ,  $\exists r > 0$ , s.t.  $\mathbb{B}_{n+m}((\mathbf{x}, \mathbf{y}), r) \cap \mathcal{C} \subseteq \mathcal{A}_0(\mathbf{x}_s, \mathbf{y}_s)$ , where  $\mathcal{C} = \{(\mathbf{x}, \mathbf{y}) \in \mathbb{R}^{n+m} \mid \mathbf{g}(\mathbf{x}, \mathbf{y}) = \mathbf{0}\}$ . See [30] [25, CH.7] for more details.

Next we discuss an important property of the solutions of boundary-layer system  $\Pi_0$ .

**Lemma 3.** For any given compact set  $\tilde{\mathcal{E}} \subseteq \Gamma_s$ ,  $\exists k, \gamma, \rho_0 > 0$ , s.t.  $\forall (\mathbf{x}_0, \mathbf{y}^*) \in \tilde{\mathcal{E}}$  and  $\mathbf{y}(0) \in \mathbb{B}_m(\mathbf{y}^*, \rho_0)$ ,

$$\|\mathbf{y}(\tau) - \mathbf{y}^*\| \leq k \|\mathbf{y}(0) - \mathbf{y}^*\| e^{-\gamma\tau} \quad (\forall \tau \geq 0)$$

where  $(\mathbf{x}_0, \mathbf{y}(\tau)) = \phi_{\Pi_0}(\tau, (\mathbf{x}_0, \mathbf{y}(0)))$ . In other words,  $\Pi_0$  is locally exponentially stable, uniformly in  $\mathbf{x} \in \tilde{\pi}_x(\tilde{\mathcal{E}})$ . See [21, P433] for more details.

In the following, we will analyze the solutions of  $\Sigma_\epsilon$  initiated in the vicinity of  $(\mathbf{x}_s, \mathbf{y}_s)$  in detail.

**Lemma 4.**  $\exists r_0 > 0$  and  $\epsilon_0 > 0$ , such that  $\mathbb{B}_{n+m}((\mathbf{x}_s, \mathbf{y}_s), r_0) \subseteq \bigcap_{0 < \epsilon \leq \epsilon_0} \mathcal{A}_\epsilon(\mathbf{x}_s, \mathbf{y}_s) \subseteq \mathcal{D}_0(\mathbf{x}_s, \mathbf{y}_s)$ .

*Proof:* See Appendix A.  $\square$

Next we focus on the dynamics of  $\Sigma_0$  and  $\Sigma_\epsilon$  near  $\Gamma_s$ .

**Lemma 5.**  $\mathcal{A}_0(\mathbf{x}_s, \mathbf{y}_s) \subseteq \operatorname{int}(\mathcal{D}_0(\mathbf{x}_s, \mathbf{y}_s)) \cap \Gamma_s$ .

*Proof:* See Appendix B.  $\square$

Last but not least, we analyze the dynamics of  $\Pi_0$  and  $\Pi_\epsilon$  in fast timescale.

**Lemma 6.**  $\forall (\mathbf{x}_0, \mathbf{y}^*) \in \Gamma_s, \forall (\mathbf{x}_0, \mathbf{y}_0) \in \mathcal{A}_F(\mathbf{x}_0, \mathbf{y}^*)$ , and  $\forall r_{F_0} > 0, \exists \epsilon_{F_0} > 0$  and  $\tilde{T}_{F_0} > 0$  (irrelevant of  $\epsilon$ ), s.t.  $\forall \epsilon \in [0, \epsilon_{F_0}]$ ,  $\phi_{\Pi_\epsilon}(\tilde{T}_{F_0}, (\mathbf{x}_0, \mathbf{y}_0)) \in \mathbb{B}_{n+m}((\mathbf{x}_0, \mathbf{y}^*), r_{F_0})$ . See [25, CH.16] for more details.

This is a simple consequence of continuous dependence of solutions of  $\Pi_\epsilon$  on parameter  $\epsilon$ , combined with the fact that  $\lim_{\tau \rightarrow +\infty} \phi_{\Pi_0}(\tau, (\mathbf{x}_0, \mathbf{y}_0)) = (\mathbf{x}_0, \mathbf{y}^*)$ .

**Theorem 2.** If a given point  $\mathbf{q}_\epsilon$  lies in the stability region of fast subsystem (16), and its projection on  $\Gamma_s$  is in the stability region of slow subsystem (17), then the solution of (14) initiated at  $\mathbf{q}_\epsilon$  will converge to  $(\mathbf{x}_s, \mathbf{y}_s)$ , as long as  $\epsilon$  is small enough. That is:

$$\bigcup_{(\mathbf{x}_0, \mathbf{y}_0) \in \mathcal{A}_0(\mathbf{x}_s, \mathbf{y}_s)} \mathcal{A}_F(\mathbf{x}_0, \mathbf{y}_0) \subseteq \mathcal{D}_0(\mathbf{x}_s, \mathbf{y}_s)$$

*Proof:*  $\forall p_* = (\mathbf{x}_{p_*}, \mathbf{y}_{p_*})$  satisfying  $(\mathbf{x}_{p_*}, \mathbf{h}_s(\mathbf{x}_{p_*})) \in \mathcal{A}_0(\mathbf{x}_s, \mathbf{y}_s)$  and  $(\mathbf{x}_{p_*}, \mathbf{y}_{p_*}) \in \mathcal{A}_F(\mathbf{x}_{p_*}, \mathbf{h}_s(\mathbf{x}_{p_*}))$ , Lemma 5 ensures that there is a compact small neighborhood  $\mathcal{N}_{p_*}$  of  $p_*$ , where  $p'_* = (\mathbf{x}_{p_*}, \mathbf{h}_s(\mathbf{x}_{p_*}))$ , s.t.  $\mathcal{N}_{p_*} \subseteq \mathcal{D}_0(\mathbf{x}_s, \mathbf{y}_s)$ . Denote  $\epsilon_* = \min_{p \in \mathcal{N}_{p_*}, p \in \bigcap_{0 < \epsilon \leq \epsilon_p} \mathcal{A}_\epsilon(\mathbf{x}_s, \mathbf{y}_s)} \epsilon_p$  (Note that a smaller  $\mathcal{N}_{p_*}$  can ensure a positive and larger  $\epsilon_*$ ). According to Lemma 6,  $\exists \epsilon_{**} > 0$  and  $\tilde{T}_{p_*} > 0$ , s.t.  $\forall \epsilon \in (0, \epsilon_{**})$ ,  $\phi_{\Sigma_\epsilon}(\epsilon \tilde{T}_{p_*}, (\mathbf{x}_{p_*}, \mathbf{y}_{p_*})) \in \mathcal{N}_{p_*}$ . Choose  $\epsilon_* = \min\{\epsilon_*, \epsilon_{**}, 1\}$ .  $\forall \epsilon \in (0, \epsilon_*)$ ,

$$\begin{aligned} & \lim_{t \rightarrow +\infty} \phi_{\Sigma_\epsilon}(t, \phi_{\Sigma_\epsilon}(\epsilon \tilde{T}_{p_*}, (\mathbf{x}_{p_*}, \mathbf{y}_{p_*}))) \\ &= \lim_{t \rightarrow +\infty} \phi_{\Sigma_\epsilon}(t, (\mathbf{x}_{p_*}, \mathbf{y}_{p_*})) = (\mathbf{x}_s, \mathbf{y}_s) \end{aligned}$$

As a result,  $p_* \in \bigcap_{0 < \epsilon \leq \epsilon_*} \mathcal{A}_\epsilon(\mathbf{x}_s, \mathbf{y}_s) \subseteq \mathcal{D}_0(\mathbf{x}_s, \mathbf{y}_s)$ . Notice that  $p_*$  is chosen arbitrarily in  $\bigcup_{(\mathbf{x}_0, \mathbf{y}_0) \in \mathcal{A}_0(\mathbf{x}_s, \mathbf{y}_s)} \mathcal{A}_F(\mathbf{x}_0, \mathbf{y}_0)$ , so that  $\bigcup_{(\mathbf{x}_0, \mathbf{y}_0) \in \mathcal{A}_0(\mathbf{x}_s, \mathbf{y}_s)} \mathcal{A}_F(\mathbf{x}_0, \mathbf{y}_0) \subseteq \mathcal{D}_0(\mathbf{x}_s, \mathbf{y}_s)$ .  $\square$

**Theorem 3.**  $\forall \mathbf{q} = (\mathbf{x}_q, \mathbf{y}_q) \in \bigcup_{(\mathbf{x}_0, \mathbf{y}_0) \in \mathcal{A}_0(\mathbf{x}_s, \mathbf{y}_s)} \mathcal{A}_F(\mathbf{x}_0, \mathbf{y}_0)$  and  $\forall \delta > 0, \exists \epsilon_\Delta > 0$ , such that  $\forall \epsilon \in (0, \epsilon_\Delta)$ , there exists a  $t_\Delta(\epsilon) > 0$  satisfying  $\overline{\lim}_{\epsilon \rightarrow 0^+} t_\Delta(\epsilon) = 0$  to make the following statement holds:

$$\|\phi_{\Sigma_\epsilon}(t, (\mathbf{x}_q, \mathbf{y}_q)) - \phi_{\Sigma_0}(t, (\mathbf{x}_q, \mathbf{h}_s(\mathbf{x}_q)))\| \leq \delta (t \geq t_\Delta).$$

This theorem indicates that the solution of (17) can be a good approximation of the solution of (14).

*Proof:* A graphical interpretation of Theorem 3 is shown in Fig. 2. First, notice that  $\mu_0$  and  $\mu_1$  in the proof of Lemma 4 can be chosen to make  $\mathbb{V}_{l_0} \subseteq \mathbb{W} \subseteq \mathbb{B}_{n+m}((\mathbf{x}_s, \mathbf{y}_s), \delta/2)$ . In addition,  $\mathcal{N}_q$  given in the proof of Theorem 2 (with  $p_*$  replaced by  $\mathbf{q}$ ) can be chosen to make

$$\begin{aligned} \mathcal{N}_q \subseteq \{(\mathbf{x}, \mathbf{y}) \in \mathbb{R}^{n+m} \mid (\mathbf{x}, \mathbf{h}_s(\mathbf{x})) \in \mathbb{B}_{n+m}(\mathbf{q}_0, \mu_{q_0}) \cap \Gamma_s, \\ \mathbf{y} \in \mathbb{B}_m(\mathbf{h}_s(\mathbf{x}), \rho_{q_0})\} \end{aligned}$$

where  $\mathbf{q}_0 = (\mathbf{x}_q, \mathbf{h}_s(\mathbf{x}_q))$ , and  $\mu_{q_0}$  and  $\rho_{q_0}$  are defined in the proof of Lemma 5 (with  $p_0$  replaced by  $\mathbf{q}$ ). Moreover, as the vector field of (15) and (17) are smooth, both  $\phi_{\Pi_\epsilon}(\tilde{T}_q, \mathbf{q})$  and  $\phi_{\Sigma_0}(\epsilon \tilde{T}_q, \mathbf{q}_0)$  are smooth function of  $\epsilon$ , where  $\tilde{T}_q$  is defined in the proof of Theorem 2 (with  $p_*$  replaced by  $\mathbf{q}$ ). Also,  $\lim_{\epsilon \rightarrow 0^+} \phi_{\Pi_\epsilon}(\tilde{T}_q, \mathbf{q}) \in \mathbb{B}_{n+m}(\mathbf{q}_0, \rho_{q_0}) \cap \mathcal{A}_F(\mathbf{q}_0)$ ,

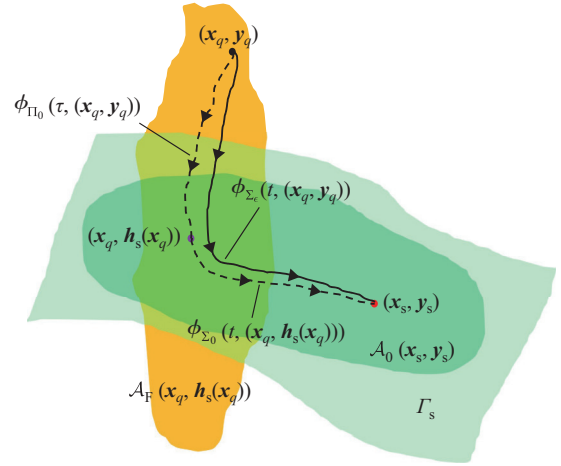


Fig. 2. A graphical interpretation of Theorem 3.

$\lim_{\epsilon \rightarrow 0^+} \phi_{\Sigma_0}(\epsilon \tilde{T}_q, \mathbf{q}_0) = \mathbf{q}_0 \in \mathbb{B}_{n+m}(\mathbf{q}_0, \rho_{q_0}) \cap \mathcal{A}_F(\mathbf{q}_0)$ . Based on Tikhonov's Theorem on Finite Interval [21, p.434], as well as the continuous dependence of solutions of (17) on initial conditions,  $\exists \epsilon_\Delta \in (0, 1)$ , s.t.  $\forall \epsilon \in (0, \epsilon_\Delta)$ ,  $\exists t_{\delta_0}(\epsilon) > 0$ , s.t.  $\forall t \in [t_{\delta_0}(\epsilon), T_{q_0}]$ ,

$$\begin{aligned} & \|\phi_{\Sigma_\epsilon}(t, \phi_{\Sigma_\epsilon}(\epsilon \tilde{T}_q, \mathbf{q})) - \phi_{\Sigma_0}(t, \mathbf{q}_0)\| \leq \delta/2 \\ & \|\phi_{\Sigma_0}(t, \phi_{\Sigma_0}(\epsilon \tilde{T}_q, \mathbf{q}_0)) - \phi_{\Sigma_0}(t, \mathbf{q}_0)\| \leq \delta/2 \\ & \phi_{\Sigma_\epsilon}(T_{q_0} + \epsilon \tilde{T}_q, \mathbf{q}) \in \mathbb{V}_{l_0}, \phi_{\Sigma_0}(T_{q_0} + \epsilon \tilde{T}_q, \mathbf{q}_0) \in \mathbb{V}_{l_0} \end{aligned}$$

where  $T_{q_0}$  is defined in the proof of Lemma 5 (with  $p_0$  replaced by  $\mathbf{q}$ ). Since  $\mathbb{V}_{l_0} \subseteq \mathbb{B}_{n+m}((\mathbf{x}_s, \mathbf{y}_s), \delta/2)$  is positively invariant,

$$\|\phi_{\Sigma_\epsilon}(t + \epsilon \tilde{T}_q, \mathbf{q}) - \phi_{\Sigma_0}(t + \epsilon \tilde{T}_q, \mathbf{q}_0)\| \leq \delta$$

for all  $t \in [t_{\delta_0}(\epsilon), +\infty]$ . Note that  $\overline{\lim}_{\epsilon \rightarrow 0^+} \epsilon \tilde{T}_q + t_{\delta_0}(\epsilon) = 0$  can be inferred from Tikhonov's Theorem. Choose  $t_\Delta(\epsilon) = \epsilon \tilde{T}_q + t_{\delta_0}(\epsilon)$ , the proof of Theorem 3 is completed.  $\square$

### E. Properties of the FOSR and ROSR

Now we return to system (1), (5) and (13) to derive the properties of the FOSR and ROSR.

**Theorem 4.**  $\forall \mathbf{x}(0) \in \mathcal{D}$ , if  $\mathbf{T}^+ \mathbf{x}(0) \in \hat{\mathcal{D}}$ , then the trajectory of (1) initiated at  $\mathbf{x}(0)$  will approach  $\mathcal{S} \triangleq \{\mathbf{x}_s \mid \mathbf{x}_s = \mathbf{Tz}, \mathbf{z} \in \mathbb{R}^r\}$  in a short period of time, and then can be well-approximated by the trajectory  $\mathbf{T} \circ \hat{\mathcal{S}}(t, \mathbf{T}^+ \mathbf{x}(0))$ .

*Proof:* A graphical interpretation of Theorem 4 is shown in Fig. 3. Since  $\mathbf{x}(0) \in \mathcal{D}$ , system (13) can be used to analyze the solution of system (1) starting at  $\mathbf{x}(0)$ . In addition, as system (5) is the slow subsystem of system (13) and  $\mathbf{T}^+ \mathbf{x}(0)$  is located in its domain of attraction, based on Theorem 3,  $\hat{\mathcal{S}}(t, \mathbf{T}^+ \mathbf{x}(0))$  is a good approximation of  $\mathbf{z}(t) = \mathbf{T}^+ \mathbf{x}(t)$ . Moreover, as  $\mathbf{x}(0) \in \mathcal{D}$ ,  $\mathbf{x}(t) = \mathbf{Tz}(t) + (\mathbf{I}_n - \mathbf{TT}^+) \bar{\omega}_f(t) + \text{errs}$  with term  $\bar{\omega}_f(t)$  and *errs* decaying rapidly. Therefore,  $\mathbf{x}(t)$  approaches  $\mathbf{Tz}(t)$  in a short period of time. Finally, because  $\mathbf{Tz}(t) \in \mathcal{S}$ ,  $\mathbf{x}(t)$  approaches  $\mathcal{S}$  rapidly, and then  $\mathbf{x}(t)$  will be approximated by  $\mathbf{T} \circ \hat{\mathcal{S}}(t, \mathbf{T}^+ \mathbf{x}(0))$  since  $\mathbf{Tz}(t)$  is well-approximated by  $\mathbf{T} \circ \hat{\mathcal{S}}(t, \mathbf{T}^+ \mathbf{x}(0))$ .  $\square$

Theorem 4 is critical, because it reveals the correspondence between the trajectory convergence behavior in the FOSR and

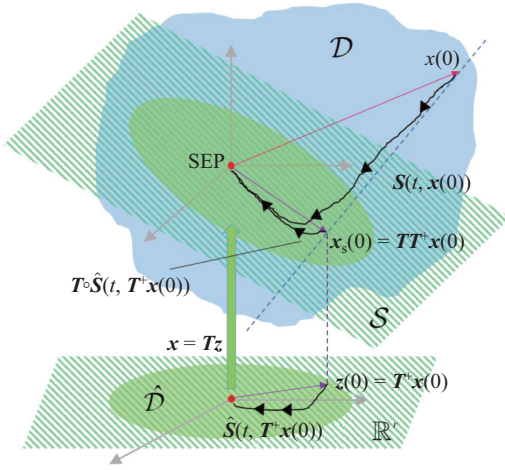


Fig. 3. A graphical interpretation of Theorem 4.

ROSR, respectively. Although  $\mathcal{D}$  and  $\hat{\mathcal{D}}$  are not topologically conjugate, Theorem 4 implies that the two are closely related and it is possible to estimate  $\mathcal{D}$  by  $\hat{\mathcal{D}}$ . Next, we will present methods to estimate the ROSR and FOSSR sequentially.

### III. MODIFIED EAD ALGORITHM TO ESTIMATE THE ROSR

In our previous work [13], an Expanding Annular Domain (EAD) algorithm combined with Sum of Squares (SOS) programming was presented to estimate the region of attraction (ROA) of a power system (referred to as the “domain of attraction” in [13]). EAD algorithm has been successfully applied on small-scale power systems. Since the reduced-order model is also low-dimensional, here we will modify EAD algorithm to estimate the ROSR.

#### A. Taylor Truncation and Polynomial System

SOS programming only discusses polynomial systems, but power systems are not modeled in polynomial form. In [13], we have proposed a coordinate transformation to turn the original non-polynomial system into a polynomial system expressed by a set of differential algebraic equations. However, the approach is not suitable for systems whose state equations contain terms  $\sin(k\delta)$  or  $\cos(k\delta)$ , where  $k$  is not an integer, such as  $\sin(0.71\delta)$ . Unfortunately, reduced-order model (5) of a typical power system has such kind of terms due to Galerkin projection. Nonetheless, we can use Taylor truncation to derive a polynomial form of the reduced-order model.

System (5) can be rewritten as:

$$\dot{z}_i = p_i(z) + \sum_{j=1}^s q_{ij}(z)\psi_{ij}(z) \quad (18)$$

where  $i = 1, 2, \dots, r$ ,  $p_i(z)$ ,  $q_{ij}(z)$  are polynomial functions,  $\psi_{ij}(z) : \mathbb{R}^r \rightarrow \mathbb{R}$  represent analytic non-polynomial functions. First, we introduce some multi-index notations:  $|\gamma| = \gamma_1 + \dots + \gamma_r$ ,  $\gamma! = \gamma_1! \dots \gamma_r!$ ,  $z^\gamma = z_1^{\gamma_1} \dots z_r^{\gamma_r}$ , where  $z \in \mathbb{R}^r$  and  $\gamma = (\gamma_1, \dots, \gamma_r)^\top \in \mathbb{N}^r$  is an  $n$ -dimensional multi-index. The  $k$ -th order mixed derivatives of  $\psi$  with respect to  $z$  can be represented as  $D^\gamma \psi = \frac{\partial \psi^{|\gamma|}}{\partial z_1^{\gamma_1} \dots \partial z_r^{\gamma_r}}$ , for some  $|\gamma| = k$ . Then,

$\psi_{ij}$  can be approximated by the truncated multi-variate Taylor expansion [31] evaluated at the origin:

$$\psi_{ij}(z) \approx \sum_{|\gamma| \leq k} D^\gamma \psi_{ij}|_{z=0} \frac{z^\gamma}{\gamma!} \quad (19)$$

which is called the  $k$ -th order Taylor truncation of  $\psi_{ij}(z)$ . Finally, from (18) and (19), we obtain a polynomial form for the reduced-order model:

$$\begin{aligned} \dot{z}_i &= p_i(z) + \sum_{j=1}^s q_{ij}(z) \left[ \sum_{|\gamma| \leq k} D^\gamma \psi_{ij}|_{z=0} \frac{z^\gamma}{\gamma!} \right] \\ &\triangleq \hat{g}_i(z), i = 1, 2, \dots, r. \end{aligned} \quad (20)$$

#### B. Boundary Constraints

Since the physical meaning of the states of the reduced-order model are no longer explicit, the estimated FOSSR derived from the obtained ROSR may violate some physical constraints:

$$|x_i| \leq \epsilon_i, \quad i = 1, 2, \dots, n \quad (21)$$

where  $\epsilon_i \in \mathbb{R}$  is a constant. When searching for the ROSR, we need to add constraints (21) to ensure that the corresponding FOSSR is within the normal range of the states of (1). From (4),  $x_i = \mathbf{E}_i \mathbf{T} z$ , where  $\mathbf{E}_i \in \mathbb{R}^{1 \times n}$  is a vector whose  $i$ -th entry is 1 and other entries are 0. According to EAD algorithm, the obtained ROSR will be denoted by  $\hat{\mathcal{D}} = \{z | \hat{V}(z) \leq 1\}$ , where  $\hat{V}(z)$  is a positive-definite SOS polynomial in  $z$ . The ROSR is required to be contained within a region that satisfies constraints (21), i.e.

$$\hat{\mathcal{D}} = \{z | \hat{V}(z) \leq 1\} \subseteq \{z | \cap_i |\mathbf{E}_i \mathbf{T} z| \leq \epsilon_i\}. \quad (22)$$

Since  $\hat{V}(z)$  only has one minimum on the boundary of the region defined by (21), (22) implies a conditional extremum problem: minimize  $\hat{V}(z)$  such that  $|\mathbf{E}_i \mathbf{T} z| = \epsilon_i$  holds for all  $i$ , and the result, denoted by  $v_m$ , is required to satisfy  $v_m \geq 1$ . The polynomial function  $\hat{V}(z)$  can be expressed as  $\hat{V}(z) = \frac{1}{2} z^\top \mathbf{P} z$  by the Square matricial representation (SMR) [11], where  $\mathbf{P} \in \mathbb{R}^{r \times r}$  is a symmetric matrix. According to the Lagrange multiplier methods [32], we have

$$H(z, \lambda) = \frac{1}{2} z^\top \mathbf{P} z + \lambda (\mathbf{E}_i \mathbf{T} z - \epsilon_i) \quad (23a)$$

$$\frac{\partial H}{\partial z}(z_m, \lambda_m) = \mathbf{P} z_m + \lambda_m (\mathbf{E}_i \mathbf{T})^\top = 0 \quad (23b)$$

$$\frac{\partial H}{\partial \lambda}(z_m) = \mathbf{E}_i \mathbf{T} z_m - \epsilon_i = 0 \quad (23c)$$

By solving equations (23b)–(23c), we obtain

$$\lambda_m = \frac{-\epsilon_i}{(\mathbf{E}_i \mathbf{T}) \mathbf{P}^{-1} (\mathbf{E}_i \mathbf{T})^\top} \quad (24a)$$

$$z_m = -\lambda_m \mathbf{P}^{-1} (\mathbf{E}_i \mathbf{T})^\top \quad (24b)$$

$$\Rightarrow v_m = \frac{1}{2} z_m^\top \mathbf{P} z_m = \frac{\epsilon_i^2}{2(\mathbf{E}_i \mathbf{T}) \mathbf{P}^{-1} (\mathbf{E}_i \mathbf{T})^\top} \quad (24c)$$

We consider the case of  $\mathbf{E}_i \mathbf{T} z = \epsilon_i$  in (23). For the case of  $\mathbf{E}_i \mathbf{T} z = -\epsilon_i$ , the result  $v_m$  is the same as (24c). Eventually, the boundary constraints can be expressed as:

$$v_m = \frac{\epsilon_i^2}{2(\mathbf{E}_i \mathbf{T}) \mathbf{P}^{-1} (\mathbf{E}_i \mathbf{T})^\top} \geq 1, \quad \forall i \in \{1, 2, \dots, n\} \quad (25)$$

### C. Modified EAD Algorithm

Combining the above results (20) and (25), we recall and improve EAD algorithm to obtain an estimated ROSR for the reduced-order model. With linear SOS programming, EAD algorithm starts from an initial estimated SR, then enlarges it by iteratively determining a series of so-called *annular domains of attraction*, each of which is characterized by the level sets of two successively obtained Lyapunov functions. See [13] for more details of EAD algorithm.

Since (20) is a system of polynomial ordinary differential equations rather than that of polynomial differential algebraic equations, the algebraic equations  $G(\mathbf{z}) = 0$  involved in [13] can be ignored. Then four SOS problems are introduced as follows.

$$\begin{aligned}
 \text{(SOSP0)} \quad & \underset{\substack{\hat{V}_0 \in \mathbb{P}_r[z], \hat{V}_0(0)=0, \\ s_1 \in \mathbb{S}_r[z]}}{\text{search}} \quad \hat{V}_0 \\
 \text{s.t.} \quad & \hat{V}_0 - q_1 \in \mathbb{S}_r[z], \\
 & -s_1(\gamma - p) - \dot{\hat{V}}_0 - q_2 \in \mathbb{S}_r[z] \tag{26}
 \end{aligned}$$

$$\begin{aligned}
 \text{(SOSP0')} \quad & \underset{s_1, s_2 \in \mathbb{S}_r[z]}{\max} \quad c \\
 \text{s.t.} \quad & -s_1(c - \hat{V}_0) - s_2 \dot{\hat{V}}_0 - q_1 \in \mathbb{S}_r[z] \tag{27}
 \end{aligned}$$

$$\begin{aligned}
 \text{(SOSP2)} \quad & \underset{s_2, s_3, s_4 \in \mathbb{S}_r[z]}{\text{search}} \quad s_2, s_4 \\
 \text{s.t.} \quad & -s_2(1 - \hat{V}^{(k)}) - s_3(\hat{V}^{(k)} - \beta) \\
 & -s_4 \dot{\hat{V}}^{(k)} - \varepsilon_2 \in \mathbb{S}_r[z] \tag{28}
 \end{aligned}$$

$$\begin{aligned}
 \text{(SOSP3)} \quad & \underset{\substack{\hat{V}^{(k+1)} \in \mathbb{P}_r[z], \hat{V}^{(k+1)}(0)=0, \\ s_1, s_3, s_5 \in \mathbb{S}_r[z]}}{\text{search}} \quad \hat{V}^{(k+1)} \\
 \text{s.t.} \quad & -s_1(1 + \varepsilon_1 - \hat{V}^{(k)}) + (1 - \hat{V}^{(k+1)}) \in \mathbb{S}_r[z] \\
 & \hat{V}^{(k+1)} - q \in \mathbb{S}_r[z], \\
 & -\bar{s}_2(1 - \hat{V}^{(k+1)}) - s_3(\hat{V}^{(k)} - \beta) \\
 & -\bar{s}_4 \dot{\hat{V}}^{(k+1)} - \varepsilon_2 \in \mathbb{S}_r[z], \\
 & -s_5(\beta - \hat{V}^{(k)}) + (\beta - \hat{V}^{(k+1)}) \in \mathbb{S}_r[z]. \tag{29}
 \end{aligned}$$

where  $q, q_1, q_2$  are given SOS polynomials with small coefficients,  $\beta$  is a given constant satisfying  $0 < \beta \leq 1$ ,  $\hat{V}^{(k)}$  is a given polynomial Lyapunov function,  $\varepsilon_{1,2} > 0$  are sufficiently small parameters,  $k$  is the iteration index of the loop.

Based on the above SOS problems, a modified EAD algorithm for the reduced-order model is shown in Algorithm 1. And we obtain an estimated ROSR:

$$\hat{D} = \{\mathbf{z} | \hat{V}_d(\mathbf{z}) \leq 1\} \tag{30}$$

where  $\hat{V}_d$  is the desired Lyapunov functions.

The differences between the original EAD algorithm and the modified one are concluded as follows.

(a) The modified EAD algorithm transforms the original non-polynomial system into a polynomial system described by

---

### Algorithm 1: Modified EAD Algorithm

---

**Input:** System (20), the degree of all assumed Lyapunov function  $\deg(\hat{V})$ , a positive definite polynomial  $p_0(\mathbf{z})$ , a positive number  $\gamma_0$ , small positive parameters  $\varepsilon_{1,2}$ , an empirical parameter  $\beta \in (0, 1]$ , the transformation matrix  $\mathbf{T}$ , physical constrains (21).

**Output:** The estimated ROSR  $\hat{D} = \{\mathbf{z} | \hat{V}_d(\mathbf{z}) \leq 1\}$ .

**Step 0:** Initialization.

**(0a)** Set  $p = p_0(\mathbf{z})$ ,  $\gamma = \gamma_0$  and solve problem SOSP0. If the problem is feasible, then save the result  $\hat{V}_0$  and go to (0b). Otherwise, reset  $\deg(\hat{V})$ ,  $p_0(\mathbf{z})$ ,  $\gamma_0$  and try (0a) again.

**(0b)** Update  $\hat{V}_0$  and perform a bisection search on  $c$  to solve problem SOSP0'. Save the resulting  $c$  as  $c_0$ . Set  $k = 1$ ,  $\hat{V}^{(1)} = \hat{V}_0/c_0$  and regard the set  $D^{(1)} := \{\mathbf{z} | \hat{V}^{(1)}(\mathbf{z}) \leq 1\}$  as an initial estimated ROSR. Then go to Step 1.

**Step 1:** Update  $\hat{V}^{(k)}$  and solve problem SOSP2. If the problem is feasible, save the resulting  $s_2, s_4$  as  $\bar{s}_2, \bar{s}_4$ , respectively, and go to Step 2.

**Step 2:** Update  $\hat{V}^{(k)}$ ,  $\bar{s}_2$  and  $\bar{s}_4$ , then solve problem SOSP3. If the problem is feasible, save the resulting  $\hat{V}^{(k+1)}$  and go to Step 3. Otherwise, go to Step 4.

**Step 3:** Set  $k = k + 1$ , and we obtain a larger estimated ROSR  $D^{(k)} := \{\mathbf{z} | \hat{V}^{(k)}(\mathbf{z}) \leq 1\}$  ( $k > 1$ ). Perform SMR for  $\hat{V}^{(k)}(\mathbf{z})$  to produce the symmetric matrix  $\mathbf{P}$ . If  $\mathbf{P}$  satisfies the boundary constrains (25), go to Step 1. Otherwise, go to Step 4.

**Step 4:** If  $k = 1$ , reset  $p_0(\mathbf{z})$ ,  $\gamma_0$ ,  $\varepsilon_{1,2}$  and  $\beta$ , then go to Step 0. If  $k > 1$ , save  $\hat{V}^{(k)}$  as  $\hat{V}_d$ , and go to Step 5.

**Step 5:** Return the estimated ROSR  $\hat{D} = \{\mathbf{z} | \hat{V}_d(\mathbf{z}) \leq 1\}$ .

---

ordinary differential equations using Taylor truncation, while the original EAD algorithm produces a polynomial differential algebraic system via a nonlinear coordinate transformation. The former is capable of considering trigonometric functions with non-integer coefficients like  $\sin(0.71\delta)$ , while the latter is not.

(b) The boundary constraints (25) are taken into account in Step 3 of the modified EAD algorithm, to ensure that the obtained ROSR is acceptable. The original EAD algorithm does not require any additional constraints for the states.

## IV. CONSTRAINED EQUIDISTANT PROJECTION TO ESTIMATE THE FOSR

After approximating the ROSR, we recast it to the full-order state space to estimate the FOSR. According to Theorem 1, all points in  $\mathcal{P}$  can be projected into  $\mathcal{Q}$ . And if  $\mathcal{Q} = \hat{D}$  is the estimated ROSR, there exists an estimated FOSR  $D$  satisfying  $D \subset \mathcal{P}$ . Thus, we will introduce a so-called *constrained equidistant projection* (CEP) to search for a  $D$  contained in  $\mathcal{P}$ .

**Definition 2.** Given three sets  $\mathcal{Q}$ ,  $\mathcal{S}$  and  $\mathcal{P}$  based on Definition 1, we define  $\mathcal{G} \triangleq \{\mathbf{x}_g | \mathbf{x}_g = \mathbf{x}_p - \mathbf{x}_s \triangleq \mathbf{G}\mathbf{x}_p, \mathbf{x}_p \in \mathcal{P}\}$  and  $\mathbf{x}_e \triangleq \frac{\|\mathbf{x}_p\|}{\|\mathbf{x}_s\|} \mathbf{x}_s$  for  $\|\mathbf{x}_s\| \neq 0$ , i.e.  $\mathbf{x}_e$  is the equidistant projection of  $\mathbf{x}_p$  on  $\mathbf{x}_s$ .

**Theorem 5.** Given an estimated ROSR  $\hat{D} = \{\mathbf{z} | \hat{V}_d(\mathbf{z}) \leq 1\}$  and a transformation  $\mathbf{x} = \mathbf{T}\mathbf{z}$ , let  $\mathcal{Q} = \hat{D}$  and from Definition 1, we have the sets  $\mathcal{S}$  and  $\mathcal{P}$ . Based on Definition 2, for system (1) and a given point  $\mathbf{x}_p$ , if

$$\hat{V}_d(\mathbf{T}^+ \mathbf{x}_e) \leq 1 \tag{31a}$$

$$\langle \mathbf{G}\mathbf{f}(\mathbf{x}_p), -\mathbf{G}\mathbf{x}_p \rangle > 0 \tag{31b}$$

the trajectory starting from  $\mathbf{x}_p$  and governed by system (1) will approach  $\mathcal{S}$  and converge to the origin.

*Proof:* Obviously, from the definition of  $\mathcal{P}$  and  $\mathcal{G}$ ,  $\mathbf{x}_s$  is the orthogonal projection of  $\mathbf{x}_p$  on manifold  $\mathcal{S}$ , and  $\mathbf{x}_g \perp \mathbf{x}_s$ . Then  $\mathbf{x}_p = \mathbf{x}_s + \mathbf{x}_g$  implies a decomposition of slow and fast modes, since trajectories on  $\mathcal{S}$  are dominated by slow modes according to Theorem 4. A graphical interpretation of Theorem 5 is shown in Fig. 4.

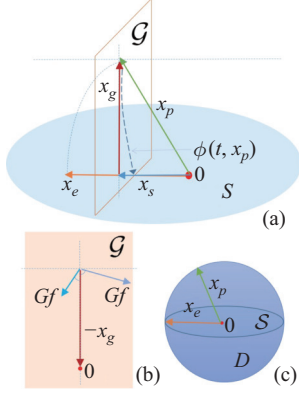


Fig. 4. A graphical interpretation of Theorem 5. (a) Equidistant projection. (b) Direction constraint. (c) A part of the estimated FOSR.

From Theorem 1,  $\mathbf{T}^+\mathbf{x}_p = \mathbf{z}_q \in \hat{D}$  and  $\mathbf{x}_g = \mathbf{x}_p - \mathbf{x}_s = (\mathbf{I} - \mathbf{T}\mathbf{T}^+)\mathbf{x}_p \triangleq \mathbf{G}\mathbf{x}_p$ . Then  $\mathbf{G} = \mathbf{I} - \mathbf{T}\mathbf{T}^+$ . Since  $\mathbf{G}\mathbf{x}_p$  denotes the projection of  $\mathbf{x}_p$  on  $\mathcal{G}$  and  $\mathbf{G}\mathbf{x}_p = \mathbf{x}_g$ , condition (31b) implies that the direction of the projection of  $\mathbf{f}(\mathbf{x}_p)$  on  $\mathcal{G}$  is toward  $\mathcal{S}$ , as shown in Fig. 4(b). Combining  $\mathbf{T}^+\mathbf{x}_p \in \hat{D}$  and Theorem 4, it follows that the trajectory starting from  $\mathbf{x}_p$  will approach  $\mathcal{S}$ .

The trajectory initiated at  $\mathbf{x}_p$  is denoted by  $\phi(t, \mathbf{x}_p)$ , and its decomposition of slow and fast modes is  $\phi(t, \mathbf{x}_p) = \phi_s(t, \mathbf{x}_s) + \phi_g(t, \mathbf{x}_g)$ . As  $\phi(t, \mathbf{x}_p)$  approaches  $\mathcal{S}$ , from the proof of Theorem 4, we know that  $\phi_g(t, \mathbf{x}_g)$  decays much faster than  $\phi_s(t, \mathbf{x}_s)$ . Assume the trajectory arrives in the vicinity of  $\mathcal{S}$  when  $t = t^*$ . Then we have  $\|\phi_s(t^*, \mathbf{x}_s)\| \approx \|\mathbf{x}_s\|$  and  $\|\phi_g(t^*, \mathbf{x}_g)\| \approx 0$ . Since  $\|\mathbf{x}_p\| = \|\mathbf{x}_e\| \geq \|\mathbf{x}_s\|$ , we have  $\|\phi(t^*, \mathbf{x}_p)\| = \|\phi_s(t^*, \mathbf{x}_s) + \phi_g(t^*, \mathbf{x}_g)\| \leq \|\mathbf{x}_s\| \leq \|\mathbf{x}_e\|$ . Because the angle between vector  $\phi(t^*, \mathbf{x}_p)$  and  $\mathbf{x}_e$  is generally small and  $\hat{V}_d(z)$  is an SOS polynomial, if  $\hat{V}_d(\mathbf{T}^+\mathbf{x}_e) \leq 1$ , we have  $\hat{V}_d(\mathbf{T}^+\phi(t^*, \mathbf{x}_p)) \leq 1$ , which guarantees that the trajectory will land within  $\mathcal{S}$ . Then from Theorem 4,  $\phi(t, \mathbf{x}_p)$  with  $t > t^*$  can be well-approximated by the projection of the related trajectory evolved in  $\hat{D}$ , and converge to the origin.  $\square$

Condition (31) can describe a part of the estimated FOSR  $D$ , as shown in Fig. 4(c). Obviously,  $D \subset \mathcal{P}$ .

According to Theorem 1, we have  $\mathbf{T}^+\mathbf{x}_e = \mathbf{T}^+\frac{\|\mathbf{x}_p\|}{\|\mathbf{x}_s\|}\mathbf{x}_s = \mathbf{T}^+\frac{\|\mathbf{x}_p\|}{\|\mathbf{x}_s\|}\mathbf{T}\mathbf{T}^+\mathbf{x}_p = \frac{\|\mathbf{x}_p\|}{\|\mathbf{x}_s\|}\mathbf{T}^+\mathbf{x}_p$  for  $\|\mathbf{x}_s\| \neq 0$ . If  $\mathbf{x}_p = \mathbf{x}_s + \mathbf{x}_g = \mathbf{x}_g$  with  $\|\mathbf{x}_s\| = 0$ , we search for a maximum  $l > 0$  by performing time domain simulation of system (1), such that

$$\lim_{t \rightarrow \infty} \phi(t, \mathbf{x}_p) = \mathbf{0}, \quad \|\mathbf{x}_p\| \leq l. \quad (32)$$

Now, we expand  $\mathcal{P}$  to the entire space, i.e.  $\mathbf{x}_p = \mathbf{x}$ , then  $\mathbf{x}_s = \mathbf{T}\mathbf{T}^+\mathbf{x}$  and  $\mathbf{T}^+\mathbf{x}_e = \frac{\|\mathbf{x}\|}{\|\mathbf{x}_s\|}\mathbf{T}^+\mathbf{x}$  are satisfied. According to Theorem 5 and (32), we have

$$\begin{cases} \hat{V}_d\left(\frac{\|\mathbf{x}\|}{\|\mathbf{x}_s\|}\mathbf{T}^+\mathbf{x}\right) \leq 1, & \|\mathbf{x}_s\| \neq 0 \\ \langle \mathbf{G}\mathbf{f}(\mathbf{x}), -\mathbf{G}\mathbf{x} \rangle > 0 \\ \|\mathbf{x}\| \leq l, & \|\mathbf{x}_s\| = 0 \end{cases}, \quad (33)$$

where  $\mathbf{G} = \mathbf{I} - \mathbf{T}\mathbf{T}^+$ . Finally, an estimated FOSR  $D$  can be expressed as:

$$D = \{\mathbf{x} | \text{condition (33) holds}\}. \quad (34)$$

The above procedure is called CEP. It utilizes an equidistant projection of  $\mathbf{x}$  and a direction constraint (31b) to restrict  $\hat{D}$ , leading to a satisfactory  $D$ . Based on Theorem 5, the result is guaranteed to be moderately conservative and fairly reliable.

Finally, we call the whole process of utilizing the modified EAD algorithm to estimate ROSR and then using the CEP to estimate FOSR as *reduced-order stability region mapping* (ROSRM) method.

## V. EXAMPLES

In this section, the proposed ROSRM method is applied to the IEEE 10-machine-39-bus power system case. The estimated FOSR is compared with that obtained by the traditional energy function method. Moreover, we use time domain simulation and introduce the *critical clearing time* (CCT) of faults [2] to verify the results.

### A. Model of IEEE 10-machine-39-bus Power System

We recall the internal node model of a  $g$ -machine power system (Generator 1 is regarded as the reference machine) introduced in Part I. Here, we will compare the ROSRM method with the energy function method [2]. To search for the UEP and construct the energy function, we have to consider the relative rotor angular velocity. Thus, we use the uniform damping ratio to further simplify the model:

$$\begin{aligned} \frac{d\delta_{i1}}{dt} &= \omega_{i1} \\ \frac{d\omega_{i1}}{dt} &= \frac{\omega_b}{2H_i}(P_{mi} - P_{ei}) - \frac{\omega_b}{2H_1}(P_{m1} - P_{e1}) - \lambda\omega_{i1} \end{aligned} \quad (35)$$

where  $i = 2, 3, \dots, g$ .  $\delta_{i1}$  represents the relative rotor angle [rad] and  $\omega_{i1}$  is the relative rotor angular velocity [rad/s].

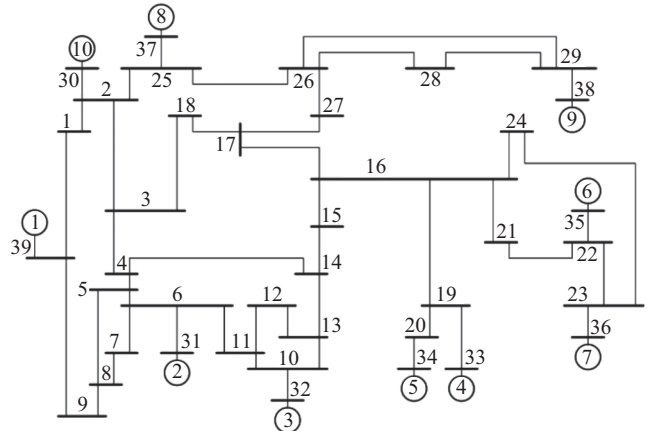


Fig. 5. One-line diagram of the IEEE 10-machine-39 bus power system.

For  $i = 1, 2, \dots, g$ ,  $P_{ei} = \sum_{j=1}^g E_i E_j \{G_{ij} \cos(\delta_{i1} - \delta_{j1}) + B_{ij} \sin(\delta_{i1} - \delta_{j1})\}$  is the electrical power [p.u.].  $E_i$ ,  $P_{mi}$  represent the internal voltage and mechanical input respectively [p.u.].  $B_{ij}$ ,  $G_{ij}$  are the susceptance and conductance between generators  $i$  and  $j$  respectively [p.u.].  $H_i$  is the time inertia constant [s],  $\lambda$  is the uniform damping ratio and  $\omega_b = 120\pi$  is the reference value of  $\omega_i$ . Electrical loads are modeled as constant impedances. For simplicity, we shift the equilibrium point of the system (35) to the origin. Assuming that  $(\delta_{21}^*, \delta_{31}^*, \dots, \delta_{g1}^*, 0, \dots, 0)$  is the stable equilibrium point, we define a new state vector  $\mathbf{x} \in \mathbb{R}^n (n = 2g - 2)$  as:

$$\begin{aligned} \mathbf{x} &= [x_1, \dots, x_{g-1}, x_g, \dots, x_n] \\ &= [\Delta\delta_{21}, \dots, \Delta\delta_{g1}, \omega_{21}, \omega_{31}, \dots, \omega_{g1}] \\ &= [\delta_{21} - \delta_{21}^*, \dots, \delta_{g1} - \delta_{g1}^*, \omega_{21}, \omega_{31}, \dots, \omega_{g1}] \end{aligned} \quad (36)$$

In this case,  $\lambda = 1.508$ ,  $g = 10$  and  $n = 18$ . More parameters are in Appendix C. From Part I, we can derive a reduced-order model based on Koopman operator. Since the relative rotor angular velocity is employed here, the obtained dominant Koopman eigenvalues do not contain real eigenvalues. Thus, the 5-order model obtained in Part I can be further simplified to a 4-order model, whose associated transformation matrix  $T$  is shown in Appendix C. Finally, the reduced-order model is described by (5), where  $r = 4$ .

### B. Comparison Between the ROSRM Method and the Energy Function Method

First, we apply the ROSRM method to estimate the ROSR and FOSR for the IEEE 10–39 power system. The full-order model is transformed into a polynomial system by 5-order Taylor truncation. The physical constraints (21) are set to  $|x_i| \leq \pi/2$  ( $i = 1, 2, \dots, 9$ ) and  $|x_i| \leq \pi$  ( $i = 10, 11, \dots, 18$ ). Additionally, by setting  $\deg(\hat{V}) = 2$ ,  $p_0(z) = \sum_{i=1}^6 z_i^2$ ,  $\gamma_0 = 1.5$ ,  $\varepsilon_1 = 10^{-4}$ ,  $\varepsilon_2 = 10^{-6}$  and  $\beta = 0.5$ , we obtain an estimate of the ROSR  $\hat{D}$  by the modified EAD algorithm (Algorithm 1) and depict its boundary in Fig. 6. Then we use CEP and the obtained  $\hat{D}$  to produce an estimated FOSR  $D$  (34), where  $l = 1.25$  is calculated by (32). The boundary of  $D$  obtained by the ROSRM method is inscribed by the red surface in Fig. 7. Note that  $D$  is a 18-dimensional manifold and to visualize it,  $D$  is projected onto the  $\Delta\delta_{21}$ - $\Delta\delta_{31}$ - $\Delta\delta_{41}$  space. The above procedure takes only 142 seconds for the IEEE 10–39 power system. The obtained  $\hat{D}$  is shown in Appendix C, and  $D$  can be easily computed from  $\hat{D}$  and (33).

The ROSRM method estimate the entire FOSR rather than the local relevant boundary of the FOSR for lossy power systems(considering transfer conductance). Among traditional methods, the Closest UEP method combined with numerical energy functions is the only one that can estimate the entire FOSR for lossy power systems [3], [33]. Therefore, we will compare the effectiveness of these two methods.

From [2], we utilize the first-integral principle and ray approximation scheme to construct a numerical energy function for the IEEE 10–39 power system (35). Finding the closest UEP is time-consuming and challenging due to the high-dimensional nature of the full-order system. Since the uniform damping ratio is employed in (35), we search for

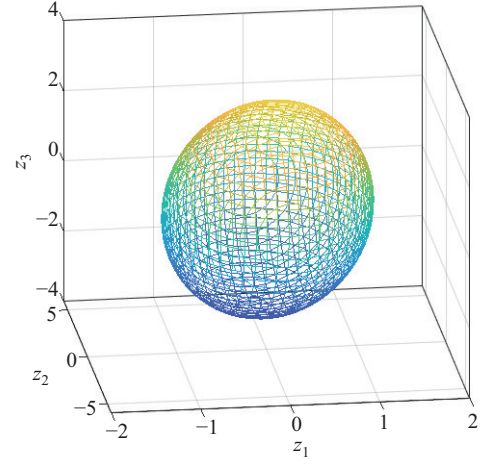


Fig. 6. The estimated ROSR projected in the  $z_1$ - $z_2$ - $z_3$  space with  $z_4 = 0.1$ .

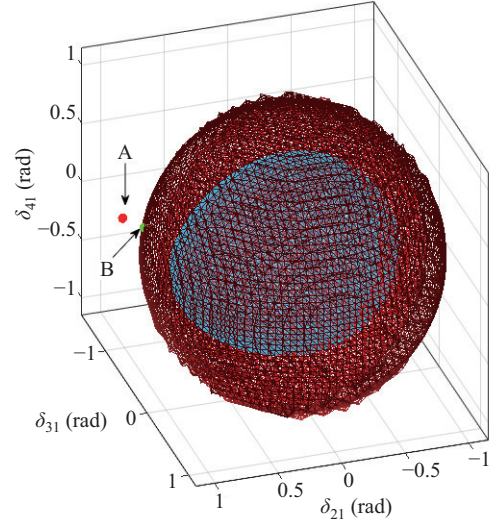


Fig. 7. The estimated FOSR projected in the  $\Delta\delta_{21}$ - $\Delta\delta_{31}$ - $\Delta\delta_{41}$  space with the other states set to 0. The red surface shows the boundary of estimated FOSR obtained by the ROSRM method, while the blue surface shows that obtained by the Closest UEP method based on numerical energy function.

the closest UEP in the subspace consisting of all  $\Delta\delta_{i1}$ . Six points are selected in each dimension, resulting in a total of  $6 \times 9$  points used as initial points to search for UEPs, which takes more than 10 hours. Here, the resulting closest UEP is  $\mathbf{x}_{cu} = [0.3585, 0.3941, 0.5283, 0.5250, 0.5230, 0.5269, 0.5096, 1.9747, 0.3789, 0, \dots, 0]$ . Finally, based on  $\mathbf{x}_{cu}$ , an estimated FOSR is computed and inscribed by the blue surface in Fig. 7.

From Fig. 7, we notice that compared with the traditional energy function method, the ROSRM method provides a less conservative result, i.e. the estimated FOSR  $D$  obtained by the latter is larger than that by the former. To verify the reliability of  $D$ , we choose two points A  $(0.8292, -1.5708, -0.3708, 0, \dots, 0)$  and B  $(1.079, -0.2812, 0.2792, 0, \dots, 0)$ . Points A and B are very close, located outside and inside  $D$  respectively. From Fig. 8, the time response of the system from initial point B converges to the equilibrium point  $\mathbf{x} = 0$ , while that from initial point A dose not. Moreover, there

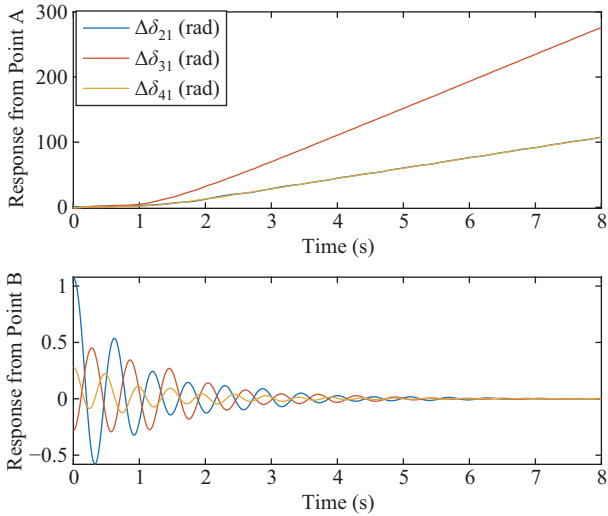


Fig. 8. Time responses of the IEEE 10–39 system from initial points A and B indicated in Fig. 7.

exist a point  $\mathbf{x}_t = [0.3586, 0.3940, 0.5282, 0.5250, 0.5230, 0.5269, 0.5096, 1.9747, 0.3789, 0, \dots, 0]$  which is within the estimated FOSR produced by the energy function method and is outside that obtained by the ROSRM method. Actually, the trajectory starting from  $\mathbf{x}_t$  is unstable, implying that the energy function method misjudges stability for  $\mathbf{x}_t$ . We summarize the differences between the two methods in Table I. These results indicate that the ROSRM method outperforms the energy function method in terms of computational speed and reliability.

TABLE I  
COMPARISON OF DIFFERENT METHODS

Methods	Cost time	Reliability of results
ROSRM method	142 s	Moderately conservative and acceptable
Energy function method	more than 10 h	Extremely conservative, unreliable

For large-scale lossy power systems, the employed numerical energy function exists inevitable numerical errors, and searching for the closest UEP has a heavy computational burden. The ROSRM method reduces the computational burden and guarantees the reliability of results by introducing the reduced-order stability region with rigorous theoretical guarantees. This is the reason why the ROSRM method is superior to the energy function method.

### C. Verification by Time Domain Simulation

For a large-scale power system, its estimated FOSR is high-dimensional and difficult to visualize. Here, we use time domain simulation and introduce the *critical clearing time* (CCT) of faults [2] to verify the results. CCT is an important metric to assess the transient stability of a power system. It is defined as the maximum allowable time from the occurrence of a fault until the fault is removed. The more stable the power system, the greater the CCT of each fault.

The real CCTs for all possible faults are calculated by time domain simulation, which requires repeatedly tracking

the fault-on and post-fault trajectories for each fault and is time-consuming in practice. Instead, we can quickly compute the CCT by simply keeping track of the time at which the fault-on trajectory reaches the boundary of the SR. The CCT based on SR is acceptable if it is smaller than and close to the real CCT. In this section, the CCTs calculated by the ROSRM method and the energy function method are shown in Table II. We notice that all the CCTs obtained by the former are larger than that computed by the latter, and are more close to the real CCTs. Therefore, compared with the energy function method, the ROSRM method is less conservative and more accurate for transient stability analysis.

TABLE II  
CCT CALCULATED BY DIFFERENT METHODS

Fault bus	Real CCT (s)	CCT by ROSRM method (s)	CCT by energy function method (s)
8	0.3103	0.1203	0.0695
23	0.2102	0.1047	0.0492
10	0.2211	0.1094	0.0539
27	0.1820	0.0992	0.0523
14	0.2398	0.1070	0.0648
18	0.2508	0.1002	0.0680
28	0.1500	0.0844	0.0430

## VI. CONCLUSION

To estimate the stability region of a large-scale power system, Part II of this paper has proposed a ROSRM method, in which a complete theory is presented to analyze the stability of the full-order model and the reduced-order model. We focus on researching the relationship between the FOSR and ROSR, by introducing singular perturbation theory and discussing the properties of the standard two timescale model. Based on the proposed theory, a modified EAD algorithm and a CEP approach are presented to estimate the ROSR and FOSR respectively. On the IEEE 10–39 power system case, the ROSRM method is demonstrated to outperform the traditional energy function method in terms of computational speed and reliability of results. Actually, the ROSRM method improves computational speed, reduces conservativeness and guarantees reliability of results, by introducing the concept of ROSR, employing SOS programming to approach the stability boundary and using CEP to screen out unstable points, respectively.

In the future, we would like to refine our work in two key directions. First, the ROSRM method will be applied to the transient stability analysis of large-scale power systems including wind farms, HVDC and energy storage, etc. Meanwhile, the effects of wind power fluctuations, LCC-HVDC commutation failures and load variations on the SR will be investigated. Second, since the ROSRM method is essentially a centralized means of analysis, it might not work well in large-scale power systems containing multiple areas. Thus, we will combine our method with connectivity-based stability methods [20]–[23] to derive a decentralized stability criterion for such cases.

## APPENDIX

### A. Proof of Lemma 4

First, since  $(\mathbf{x}_s, \mathbf{y}_s)$  is a locally exponentially stable equilib-

rium point of  $\Sigma_0$ , according to Converse Lyapunov Theorem [21, p.162-163],  $\exists \mu_0 > 0$ ,  $V \in \mathcal{C}^1(\mathbb{B}_n(\mathbf{x}_s, \mu_0); \mathbb{R})$ , and  $\alpha_1, \alpha_2, \alpha_3, \alpha_4 > 0$ , s.t.  $\forall \mathbf{x} \in \mathbb{B}_n(\mathbf{x}_s, \mu_0)$ ,

$$\begin{cases} \alpha_1 \|\mathbf{x} - \mathbf{x}_s\|^2 \leq V(\mathbf{x}) \leq \alpha_2 \|\mathbf{x} - \mathbf{x}_s\|^2 \\ \frac{\partial V}{\partial \mathbf{x}} \mathbf{f}(\mathbf{x}, \mathbf{h}_s(\mathbf{x})) \leq -\alpha_3 \|\mathbf{x} - \mathbf{x}_s\|^2 \\ \left\| \frac{\partial V}{\partial \mathbf{x}} \right\| \leq \alpha_4 \|\mathbf{x} - \mathbf{x}_s\| \end{cases} \quad (\text{A1})$$

Also,  $\mu_0$  can be chosen to make ① and ② valid.

①:  $\mathbb{B}_n(\mathbf{x}_s, \mu_0) \subseteq \tilde{\pi}_{\mathbf{x}}(\Gamma_s)$

②:  $\exists \beta_0 > 0$ , s.t.  $\forall \mathbf{x} \in \mathbb{B}_n(\mathbf{x}_s, \mu_0)$

$$\text{Re} \left\{ \text{eig} \left( \frac{\partial \mathbf{g}(\mathbf{x}, \mathbf{h}_s(\mathbf{x}))}{\partial \mathbf{y}} \right) \right\} \leq -\beta_0 < 0$$

In addition, since ② and Lemma 3 ensure that  $\Pi_0$  is locally exponentially stable, uniformly in  $\mathbf{x} \in \mathbb{B}_n(\mathbf{x}_s, \mu_0)$ , it can be inferred from Lemma 9.8 in [21] that  $\exists \mu_1 > 0$ ,  $c_1, c_2, c_3, c_4, c_5 > 0$ , and function  $W \in \mathcal{C}^1(\mathcal{W}; \mathbb{R})$ , where

$$\mathcal{W} = \{(\mathbf{x}, \mathbf{z}) \in \mathbb{R}^{n+m} | \mathbf{x} \in \mathbb{B}_n(\mathbf{x}_s, \mu_0), \mathbf{z} \in \mathbb{B}_m(\mathbf{0}, \mu_1)\}$$

s.t.  $\forall (\mathbf{x}, \mathbf{z}) \in \mathcal{W}$ ,

$$\begin{cases} c_1 \|\mathbf{z}\|^2 \leq W(\mathbf{x}, \mathbf{z}) \leq c_2 \|\mathbf{z}\|^2 \\ \frac{\partial W}{\partial \mathbf{z}} \mathbf{g}(\mathbf{x}, \mathbf{z} + \mathbf{h}_s(\mathbf{x})) \leq -c_3 \|\mathbf{z}\|^2 \\ \left\| \frac{\partial W}{\partial \mathbf{z}} \right\| \leq c_4 \|\mathbf{z}\|, \left\| \frac{\partial W}{\partial \mathbf{x}} \right\| \leq c_5 \|\mathbf{z}\|^2 \end{cases} \quad (\text{A2})$$

Furthermore, rewrite  $\Sigma_\epsilon$  as:

$$\begin{cases} \frac{d\mathbf{x}}{dt} = \mathbf{f}(\mathbf{x}, \mathbf{z} + \mathbf{h}_s(\mathbf{x})) \\ \epsilon \frac{d\mathbf{z}}{dt} = \mathbf{g}(\mathbf{x}, \mathbf{z} + \mathbf{h}_s(\mathbf{x})) - \epsilon \frac{\partial \mathbf{h}_s}{\partial \mathbf{x}} \mathbf{f}(\mathbf{x}, \mathbf{z} + \mathbf{h}_s(\mathbf{x})) \end{cases} \quad (\text{A3})$$

Define  $\nu(\mathbf{x}, \mathbf{z}) = (1-d)V(\mathbf{x}) + dW(\mathbf{x}, \mathbf{z})$ , where  $d \in (0, 1)$  is a given constant. The derivative of  $\nu$  with respect to  $t$  along the trajectories of  $\Sigma_\epsilon$  can be written as

$$\begin{aligned} \left. \frac{d\nu}{dt} \right|_{\Sigma_\epsilon} &= (1-d) \frac{\partial V}{\partial \mathbf{x}} \mathbf{f}(\mathbf{x}, \mathbf{h}_s(\mathbf{x})) \\ &+ (1-d) \frac{\partial V}{\partial \mathbf{x}} (\mathbf{f}(\mathbf{x}, \mathbf{z} + \mathbf{h}_s(\mathbf{x})) - \mathbf{f}(\mathbf{x}, \mathbf{h}_s(\mathbf{x}))) \\ &+ d \left( \frac{\partial W}{\partial \mathbf{x}} - \frac{\partial W}{\partial \mathbf{z}} \frac{\partial \mathbf{h}_s}{\partial \mathbf{x}} \right) \mathbf{f}(\mathbf{x}, \mathbf{z} + \mathbf{h}_s(\mathbf{x})) \\ &+ \frac{d}{\epsilon} \frac{\partial W}{\partial \mathbf{z}} \mathbf{g}(\mathbf{x}, \mathbf{z} + \mathbf{h}_s(\mathbf{x})) \end{aligned}$$

As set  $\mathcal{W}$  is compact, we can find positive constants  $L_1, L_2$  and  $L_3$ , such that  $\forall (\mathbf{x}, \mathbf{z}) \in \mathcal{W}$ ,

$$\begin{cases} \frac{\partial V}{\partial \mathbf{x}} (\mathbf{f}(\mathbf{x}, \mathbf{z} + \mathbf{h}_s(\mathbf{x})) - \mathbf{f}(\mathbf{x}, \mathbf{h}_s(\mathbf{x}))) \\ \leq L_1 \alpha_4 \|\mathbf{x} - \mathbf{x}_s\| \|\mathbf{z}\| \\ \left( \frac{\partial W}{\partial \mathbf{x}} - \frac{\partial W}{\partial \mathbf{z}} \frac{\partial \mathbf{h}_s}{\partial \mathbf{x}} \right) \mathbf{f}(\mathbf{x}, \mathbf{z} + \mathbf{h}_s(\mathbf{x})) \\ \leq L_2 \alpha_4 \|\mathbf{x} - \mathbf{x}_s\| \|\mathbf{z}\| + L_3 \|\mathbf{z}\|^2 \end{cases}$$

Therefore,  $\left. \frac{d\nu}{dt} \right|_{\Sigma_\epsilon} \leq -[\|\mathbf{x} - \mathbf{x}_s\|, \|\mathbf{z}\|] \mathbf{\Lambda}(d, \epsilon) [\|\mathbf{x} - \mathbf{x}_s\|, \|\mathbf{z}\|]^T$ , where

$$\mathbf{\Lambda}(d, \epsilon) =$$

$$\begin{bmatrix} (1-d)\alpha_3 & -\frac{1}{2}((1-d)L_1\alpha_4 + dL_2\alpha_4) \\ -\frac{1}{2}((1-d)L_1\alpha_4 + dL_2\alpha_4) & d\left(\frac{c_3}{\epsilon} - L_3\right) \end{bmatrix}$$

$\mathbf{\Lambda}(d, \epsilon)$  is negative definite when  $d = \frac{L_1}{L_1 + L_2}$  and  $\epsilon \in (0, \epsilon_0^*)$ , where  $\epsilon_0^* = \min\{1, \frac{\alpha_3 c_3}{\alpha_3 L_3 + L_1 L_2 \alpha_4^2}\}$ . Choose  $\epsilon_0 = 0.99\epsilon_0^*$ ,  $d = \frac{L_1}{L_1 + L_2}$  and  $l_0 = \min_{(\mathbf{x}, \mathbf{z}) \in \partial \mathcal{V}_{l_0}} \nu(\mathbf{x}, \mathbf{z})$ . Since  $\left. \frac{d\nu}{dt} \right|_{\Sigma_\epsilon} < 0$  for all  $(\mathbf{x}, \mathbf{z}) \in \mathcal{W} \setminus \{(\mathbf{x}_s, \mathbf{0})\}$  and  $\epsilon \in (0, \epsilon_0]$ , set

$$\mathcal{V}_{l_0} = \{(\mathbf{x}, \mathbf{y}) \in \mathbb{R}^{n+m} | \nu(\mathbf{x}, \mathbf{y} - \mathbf{h}_s(\mathbf{x})) \leq l_0\}$$

is positively invariant with respect to  $\Sigma_\epsilon$ . And, all trajectories of  $\Sigma_\epsilon$  initiated within  $\mathcal{V}_{l_0}$  converge to  $(\mathbf{x}_s, \mathbf{y}_s)$ . Thus,  $\mathcal{V}_{l_0} \subseteq \cap_{0 < \epsilon \leq \epsilon_0} \mathcal{A}_\epsilon(\mathbf{x}_s, \mathbf{y}_s) \subseteq \mathcal{D}_0(\mathbf{x}_s, \mathbf{y}_s)$ . Choose  $r_0 = \min_{(\mathbf{x}, \mathbf{y}) \in \partial \mathcal{V}_{l_0}} \|\mathbf{x} - \mathbf{x}_s, \mathbf{y} - \mathbf{y}_s\|^T$ , we have  $\mathbb{B}_{n+m}((\mathbf{x}_s, \mathbf{y}_s), r_0) \subseteq \mathcal{V}_{l_0} \subseteq \mathcal{D}_0(\mathbf{x}_s, \mathbf{y}_s)$ , and the proof of Lemma 4 is complete.

### B. Proof of Lemma 5

1) For any given  $p_0 \in \mathcal{A}_0(\mathbf{x}_s, \mathbf{y}_s)$ ,  $\exists T_{p_0} > 0$ , s.t.  $\phi_{\Sigma_0}(T_{p_0}, p_0) \in \mathcal{V}_{l_0/2} \cap \Gamma_s$ , where

$$\mathcal{V}_{l_0/2} = \{(\mathbf{x}, \mathbf{y}) \in \mathbb{R}^{n+m} | \nu(\mathbf{x}, \mathbf{y} - \mathbf{h}_s(\mathbf{x})) \leq l_0/2\}$$

2) Because of the continuous dependence of solutions of  $\Sigma_0$  on initial conditions and Lemma 2,  $\exists \mu_{p_0} > 0$ , s.t.  $\mathbb{B}_{n+m}(p_0, \mu_{p_0}) \cap \Gamma_s \subseteq \mathcal{A}_0(\mathbf{x}_s, \mathbf{y}_s)$ , and  $\forall p_1 \in \mathbb{B}_{n+m}(p_0, \mu_{p_0}) \cap \Gamma_s$ ,  $\phi_{\Sigma_0}(T_{p_0}, p_1) \in \mathcal{V}_{l_0/2} \cap \Gamma_s$ . Also, as both  $\Phi_{p_0, T_{p_0}}$  and  $\tilde{\pi}_{\mathbf{x}}(\Phi_{p_0, T_{p_0}})$  are compact, where

$$\Phi_{p_0, T_{p_0}} = \bigcup_{t \in [0, T_{p_0}], p_3 \in \mathbb{B}_{n+m}(p_0, \mu_{p_0}) \cap \Gamma_s} \phi_{\Sigma_0}(t, p_3)$$

$\exists \alpha_{p_0} > 0$ , s.t.  $\forall p_2 \in \Phi_{p_0, T_{p_0}}$ ,  $\text{Re}\{\text{eig}(\frac{\partial \mathbf{g}}{\partial \mathbf{y}}|_{p_2})\} \leq -\alpha_{p_0}$ .

3) Based on Lemma 3,  $\exists k_{p_0}, \gamma_{p_0}, \rho_{p_0} > 0$ , s.t.  $\forall (\mathbf{x}_0, \mathbf{y}^*) \in \Phi_{p_0, T_{p_0}}$  and  $\mathbf{y}(0) \in \mathbb{B}_m(\mathbf{y}^*, \rho_{p_0})$ ,

$$\|\mathbf{y}(\tau) - \mathbf{y}^*\| \leq k_0 \|\mathbf{y}(0) - \mathbf{y}^*\| e^{-\gamma_{p_0} \tau} \quad (\forall \tau \geq 0)$$

where  $(\mathbf{x}_0, \mathbf{y}(\tau)) = \phi_{\Pi_0}(\tau, (\mathbf{x}_0, \mathbf{y}(0)))$ .

As can be inferred from 1), 2), 3), and Tikhonov's Theorem on Finite Interval [21, p.434],  $\forall p_4 \in \mathcal{N}_{p_0}$ , where

$$\mathcal{N}_{p_0} = \{(\mathbf{x}, \mathbf{y}) \in \mathbb{R}^{n+m} | (\mathbf{x}, \mathbf{h}_s(\mathbf{x})) \in \mathbb{B}_{n+m}(p_0, \mu_{p_0}) \cap \Gamma_s, \mathbf{y} \in \mathbb{B}_m(\mathbf{h}_s(\mathbf{x}), \rho_{p_0})\}$$

$\exists \epsilon_{p_4}^* > 0$ , s.t.  $\forall \epsilon \in (0, \epsilon_{p_4}^*]$ ,  $\phi_{\Sigma_\epsilon}(T_{p_0}, p_4) \in \mathcal{V}_{l_0}$ . Choose  $\epsilon_{p_4} = \min\{\epsilon_{p_4}^*, \epsilon_0, 1\}$ . Based on Lemma 4,  $\forall \epsilon \in (0, \epsilon_{p_4}]$ ,  $\lim_{t \rightarrow +\infty} \phi_{\Sigma_\epsilon}(t, p_4) = (\mathbf{x}_s, \mathbf{y}_s)$ . Thus,  $p_4 \in \cap_{0 < \epsilon \leq \epsilon_{p_4}} \mathcal{A}_\epsilon(\mathbf{x}_s, \mathbf{y}_s) \subseteq \mathcal{D}_0(\mathbf{x}_s, \mathbf{y}_s)$ . Since  $p_4$  is chosen arbitrarily in  $\mathcal{N}_{p_0}$ ,  $\mathcal{N}_{p_0} \subseteq \mathcal{D}_0(\mathbf{x}_s, \mathbf{y}_s)$ . Finally, as  $p_0 \in \text{int}(\mathcal{N}_{p_0})$ ,  $p_0 \in \text{int}(\mathcal{D}_0(\mathbf{x}_s, \mathbf{y}_s))$ . Since  $p_0$  is chosen arbitrarily in  $\mathcal{A}_0(\mathbf{x}_s, \mathbf{y}_s)$ ,  $\mathcal{A}_0(\mathbf{x}_s, \mathbf{y}_s) \subseteq \text{int}(\mathcal{D}_0(\mathbf{x}_s, \mathbf{y}_s)) \cap \Gamma_s$ , and the proof of Lemma 5 is complete.

### C. Details of IEEE 10–39 Power System Case

Transformation matrix:

$$\mathbf{T} \in \mathbb{R}^{18 \times 4} \text{ and } \mathbf{T} =$$

$$[0.221, 0.003, 0.007, -0.022; 0.232, 0.005, 0.036, -0.026;$$

$$0.318, 0.009, -0.008, -0.043; 0.383, 0.015, -0.05, -0.071;$$

$$0.303, 0.007, 0.046, 0.003; 0.302, 0.006, 0.046, -0.028;$$

$$0.23, 0.003, -0.043, -0.033; 0.305, 0.005, -0.03, -0.065;$$

$$0.209, 0.003, -0.022, 0.002; -0.128, -0.237, -0.013, 0.04;$$

$$-0.013, -0.269, -0.242, -0.333; 0.1, -0.382, -0.218, 0.112;$$

$$0.397, -0.489, -0.459, 0.351; 0.041, -0.345, 0.378, -0.457;$$

$$-0.02, -0.332, -0.194, -0.347; -0.252, -0.26, -0.239, 0.613;$$

$$-0.134, -0.367, -0.506, 0.069; -0.094, -0.232, 0.423, 0.165]$$

where ‘;’ stands for row separator.

Parameters of the generators:

$i$	1	2	3	4	5
$H_i$ (s)	250	15.2	17.9	14.3	13
$x'_{di}$ (p.u.)	0.006	0.07	0.053	0.044	0.132
$i$	6	7	8	9	10
$H_i$ (s)	17.4	13.2	12.2	17.3	21
$x'_{di}$ (p.u.)	0.05	0.049	0.057	0.057	0.031

The estimated ROSR:  $\hat{D} = \{z | \hat{V}_d(z) \leq 1\}$ , where

$$\hat{V}_d(z) = 0.0340z_2^2 + 0.1108z_3^2 + 0.0817z_4^2 + 0.7513z_1^2$$

$$- 0.0073z_1z_2 - 0.0590z_1z_3 - 0.1603z_1z_4$$

$$+ 0.0277z_2z_3 - 0.0025z_2z_4 + 0.0114z_3z_4$$

### REFERENCES

- [1] A. H. El-Abiad and K. Nagappan, “Transient stability regions of multimachine power systems,” *IEEE Transactions on Power Apparatus and Systems*, vol. PAS-85, no. 2, pp. 169–179, Feb. 1966.
- [2] M. A. Pai, *Energy Function Analysis for Power System Stability*, New York: Springer Science & Business Media, 1989.
- [3] H. D. Chiang, *Direct Methods for Stability Analysis of Electric Power Systems: Theoretical Foundation, BCU Methodologies, and Applications*, Hoboken: John Wiley & Sons, 2011.
- [4] M. Vidyasagar, *Nonlinear Systems Analysis*, 2nd ed., Philadelphia: SIAM, 2002.
- [5] J. H. Chow, *Power System Coherency and Model Reduction*, New York: Springer, 2013.
- [6] Q. H. Wu, Y. Q. Lin, C. Hong, Y. S. Su, T. H. Wen, and Y. Liu, “Transient stability analysis of large-scale power systems: a survey,” *CSEE Journal of Power and Energy Systems*, vol. 9, no. 4, pp. 1284–1300, Jul. 2023.
- [7] G. E. Gless, “Direct method of liapunov applied to transient power system stability,” *IEEE Transactions on Power Apparatus and Systems*, vol. PAS-85, no. 2, pp. 159–168, Feb. 1966.
- [8] J. Willems, “Direct method for transient stability studies in power system analysis,” *IEEE Transactions on Automatic Control*, vol. 16, no. 4, pp. 332–341, Aug. 1971.
- [9] J. L. Willems and J. C. Willems, “The application of liapunov methods to the computation of transient stability regions for multimachine power systems,” *IEEE Transactions on Power Apparatus and Systems*, vol. PAS-89, no. 5, pp. 795–801, May 1970.
- [10] T. L. Vu and K. Turitsyn, “Lyapunov functions family approach to transient stability assessment,” *IEEE Transactions on Power Systems*, vol. 31, no. 2, pp. 1269–1277, Mar. 2016.
- [11] G. Chesi, *Domain of Attraction: Analysis and Control Via SOS Programming*, London: Springer Science & Business Media, 2011.
- [12] M. Anghel, F. Milano, and A. Papachristodoulou, “Algorithmic construction of liapunov functions for power system stability analysis,” *IEEE Transactions on Circuits and Systems I: Regular Papers*, vol. 60, no. 9, pp. 2533–2546, Sep. 2013.
- [13] Y. Q. Lin, T. H. Wen, Y. Liu, and Q. H. Wu, “Expanding annular domain algorithm to estimate domains of attraction for power system stability analysis,” *CSEE Journal of Power and Energy Systems*, vol. 10, no. 5, pp. 1925–1934, Sep. 2024.
- [14] N. G. Bretas and L. F. C. Alberto, “Lyapunov function for power systems with transfer conductances: extension of the invariance principle,” *IEEE Transactions on Power Systems*, vol. 18, no. 2, pp. 769–777, May 2003.
- [15] H. D. Chiang, “Analytical results on the direct methods for power system transient stability analysis,” *Control and Dynamic Systems: Advances in Theory and Application*, vol. 43, pp. 275–334, 1991.
- [16] T. Athay, R. Podmore, and S. Virmani, “A practical method for the direct analysis of transient stability,” *IEEE Transactions on Power Apparatus and Systems*, vol. PAS-98, no. 2, pp. 573–584, Mar. 1979.
- [17] H. D. Chiang and C. C. Chu, “Theoretical foundation of the BCU method for direct stability analysis of network-reduction power system models with small transfer conductances,” *IEEE Transactions on Circuits and Systems I: Fundamental Theory and Applications*, vol. 42, no. 5, pp. 252–265, May 1995.
- [18] H. D. Chiang, F. F. Wu, and P. P. Varaiya, “Foundations of the potential energy boundary surface method for power system transient stability analysis,” *IEEE Transactions on Circuits and Systems*, vol. 35, no. 6, pp. 712–728, Jun. 1988.
- [19] A. Llamas, J. De La Ree Lopez, L. Mili, A. G. Phadke, and J. S. Thorp, “Clarifications of the BCU method for transient stability analysis,” *IEEE Transactions on Power Systems*, vol. 10, no. 1, pp. 210–219, Feb. 1995.
- [20] F. N. Bailey, “The application of liapunov’s second method to interconnected systems,” *Journal of the Society for Industrial and Applied Mathematics, Series A: Control*, vol. 3, no. 3, pp. 443–462, Jan. 1965.
- [21] H. K. Khalil, *Nonlinear Systems*, 3rd ed., Upper Saddle River, NJ, USA: Prentice Hall, 2002.
- [22] P. Yang, F. Liu, Z. J. Wang, and C. Shen, “Distributed stability conditions for power systems with heterogeneous nonlinear bus dynamics,” *IEEE Transactions on Power Systems*, vol. 35, no. 3, pp. 2313–2324, May 2020.
- [23] B. Y. Qin, X. M. Zhang, J. Ma, S. W. Mei, and D. J. Hill, “Local input to state stability based stability criterion with applications to isolated power systems,” *IEEE Transactions on Power Systems*, vol. 31, no. 6, pp. 5094–5105, Nov. 2016.
- [24] Y. Zou, M. H. Yin, and H. D. Chiang, “Theoretical foundation of the controlling uep method for direct transient-stability analysis of network-preserving power system models,” *IEEE Transactions on Circuits and Systems I: Fundamental Theory and Applications*, vol. 50, no. 10, pp. 1324–1336, Oct. 2003.
- [25] H. D. Chiang and L. F. C. Alberto, *Stability Regions of Nonlinear Dynamical Systems: Theory, Estimation, and Applications*, Cambridge: Cambridge University Press, 2015.
- [26] C. L. DeMarco and A. R. Bergen, “Application of singular perturbation techniques to power system transient stability techniques,” California Univ., Berkeley, Tech. Rep. No. UCB/ERL M84/7, 1984.
- [27] J. D. Meiss, *Differential Dynamical Systems*, Philadelphia: SIAM, 2007.
- [28] P. Holmes, J. L. Lumley, G. Berkooz, and C. W. Rowley, *Turbulence, Coherent Structures, Dynamical Systems and Symmetry*, Cambridge: Cambridge University Press, 2012.
- [29] A. Chatterjee, “An introduction to the proper orthogonal decomposition,” *Current Science*, vol. 78, no. 7, pp. 808–817, Apr. 2000.
- [30] V. Venkatasubramanian, H. Schattler, and J. Zaborsky, “Dynamics of large constrained nonlinear systems—a taxonomy theory [power system stability],” *Proceedings of the IEEE*, vol. 83, no. 11, pp. 1530–1561, Nov. 1995.
- [31] D. K. Han, A. El-Guindy, and M. Althoff, “Power systems transient stability analysis via optimal rational liapunov functions,” in *2016 IEEE Power and Energy Society General Meeting (PESGM)*, 2016, pp. 1–5.
- [32] D. P. Bertsekas, *Constrained Optimization and LAGRANGE Multiplier Methods*, New York: Academic Press, 2014.
- [33] H. D. Chiang and J. S. Thorp, “The closest unstable equilibrium point method for power system dynamic security assessment,” in *26th IEEE Conference on Decision and Control*, 1987, pp. 72–76.



**Yuqing Lin** received a B.E. degree in Electrical Engineering from South China University of Technology, Guangzhou, China, in 2019. He is currently pursuing the Ph.D degree in South China University of Technology. His research interests include power system transient stability analysis, control of wind power generation systems, and model reduction.



**Yang Liu** received a B.E. degree and a Ph.D degree in Electrical Engineering from South China University of Technology (SCUT), Guangzhou, China, in 2012 and 2017, respectively. He is currently a Lecturer in the School of Electric Power Engineering, SCUT. His research interests include the areas of power system stability analysis and control, control of wind power generation systems, and nonlinear control theory. He has authored or co-authored more than 30 peer-reviewed SCI journal papers.



**Tianhao Wen** received a B.E. degree in Electrical Engineering from Huazhong University of Science and Technology (HUST), Wuhan, China in 2018. He obtained a Ph.D degree in South China University of Technology, Guangzhou, China, in 2023. His research interests include nonlinear observers, power system transient stability analysis and control.



**Qing-Hua Wu** received an M.Sc. degree in Electrical Engineering from Huazhong University of Science and Technology, Wuhan, China, in 1981, and a Ph.D. degree in Electrical Engineering from the Queen's University of Belfast (QUB), Belfast, U.K., in 1987. He worked as the Chair Professor at Liverpool University from 1995 to 2012. He is currently a Distinguished Professor and the Director of Energy Research Institute, South China University of Technology, Guangzhou, China. He is a Life Fellow of IEEE, Fellow of IET, CSEE Fellow, Fellow of AAIA, and Chartered Engineer. He has authored and coauthored more than 400 journal papers, 20 book chapters and 5 research monographs published by Springer Nature. His research interests include nonlinear adaptive control, mathematical morphology, artificial intelligence, and power system control and operation.



**Lei Chen** is currently pursuing a Ph.D. degree in Electrical Engineering at South China University of Technology, Guangzhou, China. His research interests include power system transient voltage stability analysis and power system planning and operation.